HHS Public Access

Author manuscript

Neuron. Author manuscript; available in PMC 2024 March 15.

Published in final edited form as:

Neuron. 2023 March 15; 111(6): 874–887.e8. doi:10.1016/j.neuron.2022.12.025.

Humidity sensors that alert mosquitoes to nearby hosts and egg-laying sites

Willem J. Laursen,

Gonzalo Budelli[†],

Ruocong Tang,

Elaine C. Chang,

Rachel Busby,

Shruti Shankar,

Rachel Gerber,

Chloe Greppi[‡],

Rebecca Albuquerque,

Paul A. Garrity[*]

Department of Biology and Volen Center for Complex Systems, Brandeis University, Waltham, MA 02453, USA.

Summary:

To reproduce and to transmit disease, female mosquitoes must obtain blood meals and locate appropriate sites for egg laying (oviposition). While distinct sensory cues drive each behavior, humidity contributes to both. Here we identify the mosquito's humidity sensors (hygrosensors). Using generalizable approaches designed to simplify genetic analysis in non-traditional model organisms, we demonstrate that the Ionotropic Receptor *Ir93a* mediates mosquito hygrosensation as well as thermosensation. We further show that *Ir93a*-dependent sensors drive human host proximity detection and blood feeding behavior, consistent with the overlapping short-range heat and humidity gradients these targets generate. After blood feeding, gravid females require *Ir93a* to seek high humidity associated with preferred egg laying sites. Reliance on *Ir93a*-dependent

[*]Correspondence: Paul Garrity, pgarrity@brandeis.edu.

[†]Current address: Department of Biophysics, Universidad de la República School of Medicine, Montevideo, 11800, Uruguay.

[‡]Current address: Department of Biological Sciences, Columbia University, New York, NY 10027, USA.

Author Contributions: W.J.L, G.B., R.T., E.C.C., R.B., S.S., and P.A.G. designed experiments. W.J.L, E.C.C., R.B., R.A. and R.G. performed husbandry, genetics and behavior. W.J.L performed molecular biology and gene targeting. W.J.L., R.T. and C.G performed immunohistochemistry. G.B. performed electrophysiology, G.B. and W.J.L. performed calcium imaging. S.S. performed RNA in situ hybridization, W.J.L., G.B., R.A. and P.A.G. performed data analysis. W.J.L. and P.A.G. created the figures and wrote the paper, with input from all authors.

Declaration of interests: P.A.G. is a co-inventor on patent WO2017196861A1 (WIPO PCT; pending; inventors: Z. Knecht, P. Garrity, L. Ni) "Methods for modulating insect hygro- and/or thermosensation". This patent proposes using members of the Ionotropic Receptor family as targets for strategies to disrupt hygro- and thermo-sensation in insects. W.J.L and P.A.G. are co-inventors on patent application PCT/US2021/052374, "Sterile organisms, methods of making, and methods of use thereof". This patent includes methods for genetic manipulations in non-traditional model organisms.

sensors to promote blood feeding and locate potential oviposition sites is shared between the malaria vector *Anopheles gambiae* and arbovirus vector *Aedes aegypti*. These *Ir93a*-dependent systems represent potential targets for efforts to control these human disease vectors.

Graphical Abstact

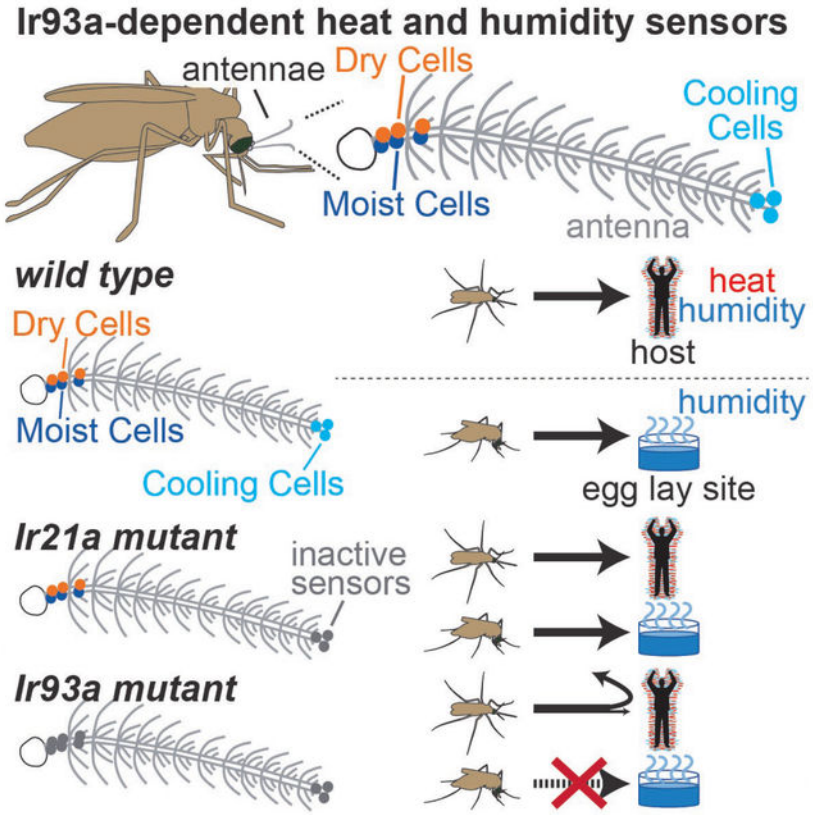

eTOC blurb:

To reproduce and spread disease, mosquitoes must blood feed and then oviposit near water – behaviors promoted by humidity sensing. Laursen et al. identify this modality's cellular and molecular basis, and show that Ionotropic Receptor *Ir93a* mediates both humidity and heat detection in mosquitoes, supporting blood feeding and oviposition site location.

Keywords

Mosquito; Anopheles gambiae; Aedes aegypti; host seeking; blood feeding; oviposition; thermosensation; hygrosensation; humidity; vector

Introduction:

Mosquitoes transmit parasites and viruses responsible for devastating diseases that sicken >500 million people and kill >500 thousand people annually [1]. For example, *Anopheles gambiae* (*An. gambiae*) mosquitoes are major vectors for human malaria in sub-Saharan

Africa, while *Aedes aegypti* (*Ae. aegypti*) mosquitoes are major vectors for dengue, Zika and other arboviruses worldwide [1–4]. The ability of female mosquitoes to seek out vertebrate hosts and feed on their blood is critical for the spread of disease, contributing to the cycle of transmission in multiple ways. Females must consume a blood meal to obtain the nutrients they need to reproduce [5]. It is also through the act of blood feeding that female mosquitoes first acquire pathogens from an infected host, and later transmit these pathogens to another host [6]. Its multiple contributions to disease transmission and vector reproduction mean that even modest reductions in blood feeding can significantly reduce disease burden, with models suggesting a two-fold decrease in blood-feeding rate can elicit an ~8-fold drop in the reproductive ratio (R value) of a vector-borne disease [7].

Host seeking and blood feeding are driven by multiple host-associated cues: visual, chemical, and physical [8–10]. Visual and chemical cues can impact mosquito behavior from meters away, but physical cues like temperature are encountered near the host, where they promote host-proximal behaviors like landing and probing [8,9]. In the malaria vector *An. gambiae*, the Ionotropic Receptor (IR) *Ir21a* was recently shown to mediate detection of host-associated temperatures [11]. But while loss of *Ir21a* impaired heat seeking, attraction to a human hand was largely unaffected [11]. One possible explanation for the persistence of host attraction in a heat-seeking defective mutant is that another, parallel short-range cue emanates from the host.

In addition to short-range thermal gradients, humans also generate short-range humidity gradients. The two gradients are largely coextensive and form a “boundary layer” of heated, moistened air that surrounds the human body [12,13], making humidity a candidate for this parallel cue (Figures 1A and 1B). While humidity sensation (hygrosensation) has been shown to promote host seeking in vector mosquitoes, both in the lab and in the field [14–17], the sensory structures, neurons, and molecular receptors involved in mosquito hygrosensation have remained unknown [18].

Compared to other modalities used in host sensing, like olfaction and vision, our understanding of humidity sensing is limited. Studies in insects whose humidity-sensing sensilla are external and accessible for electrophysiology (e.g., stick insects) have described hygrosensory sensilla containing a dry air-activated Dry Cell and a moist air-activated Moist Cell [19–22]. Similar Dry Cell/Moist Cell pairs have been identified in the *Drosophila melanogaster* antenna and found to mediate hygrosensory behaviors [23–26]. Notably, these *Drosophila* hygrosensors had eluded prior characterization due to their inaccessibility --- they reside deep within the antenna, where a cluster of ~13 hygrosensory sensilla line a large pit with a tiny (~5 micron) external opening [27,28]. In mosquitoes, some surveys have reported water vapor-activated neurons in external grooved peg sensilla [29,30], although their functional significance as hygrosensors has been debated [18,31]. To date, no canonical Moist Cell/Dry Cell pairs have been described in the mosquito, raising the question of whether they are present in the mosquito and contribute to mosquito hygrosensation.

At the molecular level, *Drosophila* hygrosensation involves receptors that, like *Ir21a*, belong to the IR family: Moist Cells require *Ir68a* and Dry Cells require *Ir40a* [23–26]. Both classes of hygrosensors also require *Ir93a*, a co-receptor that acts alongside stimulus-specific IRs

like *Ir68a* and *Ir40a* [23–25]. In *Drosophila*, *Ir93a* also acts with the fly ortholog of *Ir21a* to mediate thermosensing [32]. Although *Drosophila* do not blood feed and diverged from mosquitoes ~250 million years ago [3,33], these findings suggested that the mosquito ortholog of *Ir93a* might provide not only a means to identify the mosquito hygrosensory system, but also a single gene target whose inactivation could disrupt multiple heat- and humidity-sensing systems involved in sensing host proximity. In this way, the disruption of *Ir93a* might overcome functional redundancies among sensory modalities to interfere with host proximity detection.

In addition to helping female mosquitoes acquire a blood meal, hygrosensation is also important for egg laying. Mosquito larvae are aquatic [34], and female mosquitoes carrying mature eggs (gravid females) use hygrosensation to seek out water to lay their eggs [35,36]. Once near a pool of water, additional sensory cues, including contact with liquid water, then mediate egg deposition [37]. Oviposition sites vary among species. In *An. gambiae*, larvae frequently develop in confined pools associated with grassy vegetation near rivers [38]. In contrast, *Ae. aegypti* commonly lay eggs in small water-filled containers, including bottles, buckets, and discarded tires [39]. Such containers are common near human dwellings and appear to contribute to *Ae. aegypti*'s ability to spread globally and to thrive in urban areas [40].

Here we identify the mosquito's humidity sensors (hygrosensors), and demonstrate that the Ionotropic Receptor *Ir93a* is required for hygrosensation as well as thermosensation in mosquitoes. Using readily generalizable approaches designed to simplify genetic analysis in non-traditional model organisms, we perform parallel studies to examine *Ir93a* function in the malaria vector *An. gambiae* and the arbovirus vector *Ae. aegypti*. We demonstrate that *Ir93a* is required by both of these vector species to maintain attraction to a human host, feed efficiently on warm blood and locate appropriate sites for egg laying. Thus, we find that *Ir93a*-dependent sensory systems mediate behaviors essential for disease transmission and reproduction by two major mosquito vectors of human disease.

Results

Distinguishably Marked Knock-in Pairs (DMKPs) facilitate genetic analysis of *AgIr93a*

An. gambiae Ir93a was disrupted by CRISPR/Cas9-aided integration of a knock-in cassette into exons encoding regions important for IR function [23,24,32,41,42], the pore (*AgIr93a*^{pore} alleles) and second transmembrane domain (*AgIr93a*^{TM2} alleles) (Figure 2A). As in other nontraditional model organisms, mosquito genetic analysis is complicated by the lack of marked balancer chromosomes [43], and commonly used alternative genotyping strategies (PCR- or fluorescence intensity-based) are cumbersome or unreliable. To address this challenge, we created distinguishably marked knock-in pairs (DMKPs) by generating two knock-ins, one RFP-labeled and one EYFP-labeled, at each nucleotide position targeted by CRISPR/Cas9 (Figures 2A and 2B). The absence of nucleotides between the two insertion site positions precludes recombination between the insertions, even at scale. This permits long-term maintenance of strains carrying both insertions, and it allows unambiguous and non-invasive identification of hetero-allelic mutant animals by their distinctive two-color labeling (Figures 2C and 2D).

Unless otherwise noted, studies were performed using hetero-allelic mutants, e.g., *AgIr93a*^{pore} analyses used *AgIr93a*$^{pore\text{-}RFP}$/*AgIr93a*$^{pore\text{-}EYFP}$ animals. DMKP enabled the analysis of mutations challenging to maintain as homozygous mutant stocks (e.g., strains that blood feed poorly) and the use of genetically encoded tools (e.g., GCaMP) in mutant backgrounds. DMKP use also simplified homozygous mosquito stock generation (Figure 2E). As demonstrated below for *Aedes aegypti*, the DMKP strategy is generalizable to other species, and it should be useful for others studying diverse nontraditional model organisms, both for mutant analyses and maintenance and use of knock-in transgenes. Importantly, beyond the need to create a pair of homology-directed repair (HDR) plasmids, DMKP involves no additional effort compared to traditional knock-in approaches, as the HDR plasmids can be co-injected without issue.

AgIr93a is expressed in sensory neurons in the antenna

The *AgIr93a* knock-ins express the QF2 transcriptional activator under endogenous *AgIr93a* regulatory element control. Consistent with RNA-seq studies [44], *AgIr93a* expression was specifically detected in the antenna (Figures 3A, 3B; Figure S1A–E). Reporter [45] fidelity was confirmed by RNA in situ (Figures 3A and 3B)). *AgIr93a* expression was detected in each antennal segment (flagellomere) (Figure S1), and included neurons innervating “peg-in-pit” (coeloconic) sensilla in flagellomere 13, which contain thermosensors (Figure 3A), and in ~4 neurons per flagellomere which innervate “sharp hair” (trichoid) sensilla and co-express the olfactory co-receptor Orco (Figures S1E and S1F).

AgIr93a expression reveals *Ir93a*-dependent hygrosensors in the sensilla ampullacea

AgIr93a expression was also detected in pairs of neurons innervating a class of ~9 functionally uncharacterized sensilla in flagellomeres 1 and 2, the “peg-in-tube” sensilla ampullacea (Figure 3C, Figure S1B). Sensilla ampullacea are recessed within the antenna, at the base of a tube that extends to a small (<500 nm) opening on the underside of the antennal surface (Figure 3C)[18]. The sensilla ampullacea’s recessed location has traditionally rendered this class of sensilla inaccessible for electrophysiology and even hard to identify in anatomical surveys [46]. Thus, its function has not been previously examined. Traditionally, sensilla ampullacea have been classified as thermosensory, as they are internal and lack pores for chemical entry [18]. But as hygrosensory neurons in other insects innervate poreless sensilla [19] and can be internal [23,25], we hypothesized they might contain hygrosensors.

Using the genetic access provided by the *AgIr93a* knock-ins, the hygrosensory responses of sensilla ampullacea-innervating neurons were monitored using the genetically encoded calcium sensor GCaMP6f [47] (Figures 4A–D). In control animals (containing one wild type *AgIr93a* allele), the two neurons in each pair of *AgIr93a>GCaMP6f*-labeled neurons showed opponent responses to humidity: one neuron, the Moist Cell, was activated by humid air (as indicated by the increase in GCaMP fluorescence), and the other, the Dry Cell, was activated by dry air (Figures 4B–D). In *AgIr93a* mutants, both responses were dramatically reduced (Figures 4B–D). Thus, the sensilla ampullacea harbor hygrosensors, and these hygrosensors are *AgIr93a*-dependent.

AgIr93a is also required for mosquito thermosensing

As *AgIr93a* is also expressed in thermosensory sensilla at the antennal tip, we tested whether *AgIr93a* also mediates thermosensing, examining *AgIr21a*-dependent antennal Cooling Cells using electrophysiology (Figure 4E) [11]. Cooling Cells exhibit baseline spiking at constant temperature, and their spike rates transiently rise upon cooling and fall upon warming (Figures 4F and 4G) [11]. Similar to *AgIr21a* mutants [11], Cooling Cell thermosensitivity was abolished in *AgIr93a* mutants (Figures 4F–H), confirming *AgIr93a* acts alongside *AgIr21a* in thermosensation.

AgIr93a is required for efficient humidity and heat seeking

Having established the requirement for *AgIr93a* in humidity and temperature detection, we examined its behavioral roles. Humidity seeking was examined by providing mated, non-blood-fed females a choice between two trays, one dry and one containing water; both were mesh-covered, preventing liquid contact, but permitting water vapor escape (Figure 5A). Wild type mosquitoes preferentially accumulated on the water-containing tray, but this preference was greatly reduced in *AgIr93a* mutants (Figures 5B and 5C). In contrast, *AgIr21a* mutants, which are heat seeking-defective [11], showed no significant decrement in humidity seeking (Figures 5B and 5C). As an internal control, we confirmed that all genotypes took flight in response to human breath at the assay's end (Figure S2A). This confirmed that the mosquitoes were indeed capable of responding to other sensory cues, and that they remained so throughout the assay.

AgIr93a's contribution to heat seeking was also tested. Introduction of 4% CO_2 for 20 sec (simulating breath) prompts a subset of the mated, non-blood-fed females to take flight and participate in the heat seeking assay (Figures 5D and 5E; Figure S2B). In wild type, ~50% of these "activated" animals landed on the 37°C target, largely ignoring an adjacent 26°C target (Figures 5F and 5G). *AgIr93a* was important for heat seeking, as only ~10% of activated *AgIr93a* mutants landed on the 37°C target (Figures 5F and 5G), a defect resembling that of *AgIr21a* mutants [11].

AgIr93a-dependent sensors sustain host attraction

Having established *AgIr93a*'s importance for detecting and responding to heat and humidity presented in isolation, *AgIr93a*'s function was examined in the more complex sensory environment near a human host. Mated, non-blood-fed females were placed in a mesh cage, activated by five breaths, and presented a human hand ~3 mm above the cage (Figure 6A). This gap prevents physical contact with host, but allows exposure to host-generated chemical, visual, thermal and hygrosensory cues. ~70% of wild type mosquitoes approached and landed below the hand, sustaining their attraction for many minutes (Figures 6B–E, Movie 1). Upon hand removal, mosquitoes rapidly departed (Figure 6B; Movie 1), indicating their continued presence depended on detecting cues from the hand.

In *AgIr93a* mutants, initial host attraction was not significantly different from that of wild type (Figures 6B and 6D; Movie 2). The ability of a similar fraction of mutant mosquitoes to reach the area under the hand within 60 sec demonstrates the mutants do not exhibit general sensory behavior deficits. They remain fully capable of responding rapidly to breath and

other (*Ir93a*-independent) host stimuli in this assay, and are able to fly, orient towards and land beneath the hand. Importantly, however, the numbers of *AgIr93a* mutant mosquitoes landed beneath the hand steadily declined to well below wild type levels over the course of the assay (Figures 6B, 6D, and 6E; Movie 2, Dataset S1). Furthermore, this decline was commonly accompanied by an increase in *AgIr93a* mutants engaged in sustained flights within the cage (Figures 6C, 6F; Movie 2), suggesting these animals remain engaged in host seeking despite not landing below the hand presented. This contrasts with *AgIr21a* mutants, which sustain attraction to the hand normally [11]. These data are consistent with *AgIr93a*'s role extending beyond *AgIr21a*-dependent thermosensing to the detection of additional short-range cues that signal host proximity. Thus, *AgIr93a* is not required for initial host approach in this assay, in which longer range cues from the host are also present, but rather for sustaining close-range host attraction.

AgIr93a-dependent sensors promote blood feeding

As short-range interactions are vital for blood feeding, the consumption of a human blood meal from a collagen membrane feeder was also examined (Figure 6G). We previously showed that, when provided a choice between blood meals of differing temperature, the loss of *AgIr21a* decreased the preference of female mosquitoes for warmer over cooler blood meals [11]. However, when presented only a 37°C meal (Figure 6G), we found that *AgIr21a* mutant consumption was not significantly altered compared to wild type (Figure 6H). This indicates that although *AgIr21a*-dependent thermosensing promotes blood feeding, other sensory pathways suffice in *AgIr21a*'s absence. In contrast, blood feeding was strongly reduced in *AgIr93a* mutants: ~70% of wild type mosquitoes consumed the 37°C blood meal, compared to only ~10 to ~20% of *AgIr93a* mutants (Figure 6H). Thus, *AgIr93a* loss impairs sustained host attraction as well as membrane blood feeding, while *AgIr21a* loss impairs neither.

Like human hosts, 37°C collagen membrane feeders generate spatially overlapping temperature and humidity gradients (Figure 1B, Figure S3A). Using either room temperature blood or a water vapor impermeable membrane decreased feeding from an artificial feeder, and using both abolished feeding (Figure S3B). These data are consistent with parallel contributions of heat and humidity, although changes to the blood temperature and feeding membrane could also affect additional cues.

AgIr93a promotes water seeking by gravid females

Beyond the role of hygrosensation in helping *An. gambiae* acquire a blood meal to complete oogenesis, hygrosensation also helps gravid females seek out water to lay the resulting eggs, key for survival of their aquatic offspring [35,36]. To assess the potential for *AgIr93a* to also contribute to this behavior, the water seeking ability of gravid females, assayed 2 days after being blood fed, was tested. Consistent with *AgIr93a* also contributing to this behavior, the loss of *AgIr93a* dramatically reduced humidity seeking by gravid *An. gambiae* females compared to wild type (Figures 5B and 5C).

Examining *Ir93a* function in *Ae. aegypti*

There are two subfamilies of vector mosquitoes, Anophelinae and Culicinae, with the latter including Culex and Aedes species (Figure 7A). Anophelinae and Culicinae diverged ~180 million years ago [3]. As *Ir93a* and its IR partners are conserved across both subfamilies [42], this raises the possibility that vectors in each subfamily employ these receptors for host seeking, blood feeding and oviposition. To test this directly, we examined *Ir93a* expression and function in *Ae. aegypti*, a major vector for dengue, Zika and other arboviruses [1–4].

Two independent knock-in/disruption alleles of *Ae. aegypti Ir93a* (*AaIr93a*) were created by CRISPR-Cas9-mediated integration of a knock-in cassette upstream of the ion pore coding sequence (Figure S4A). These insertions disrupt the *AaIr93a* gene and place QF2 under control of *AaIr93a* regulatory sequences (Figure S4A). Both alleles yielded QF2-dependent reporter expression consistent with *AaIr93a* RNA expression as detected by in situ hybridization (Figure 7B). Consistent with thermo- and hygro-sensory roles, like in *An. gambiae*, *AaIr93a* expression was detected in neurons innervating coeloconic sensilla in flagellomere 13 and sensilla ampullacea in flagellomeres 1 and 2 (Figure 7B). *AaIr93a* was also detected in up to four Orco-positive neurons in other flagellomeres and, unlike *An. gambiae*, in ~7 Orco-positive neurons in the maxillary palps (Figures S4B–D). GCaMP7s [48] expression under *AaIr93a* knock-in control permitted imaging of flagellomere 13 thermosensor activity, but was too weak to reliably monitor sensilla ampullacea-associated neurons in the thicker flagellomeres 1 and 2 in live samples. In controls (containing one wild type *AaIr93a* allele), flagellomere 13 *AaIr93a>GCaMP7s* thermosensors were cooling-activated and heating-inhibited, similar to *An. gambiae* Cooling Cells (Figure S5A). Their thermosensitivity was dramatically reduced in homozygous *AaIr93a* mutants, indicating similar dependence on *Ir93a* in both species (Figure S5A).

AaIr93a mediates host sensing and blood feeding in *Ae. aegypti*

The importance of *Ir93a* for host sensing and blood feeding in *Ae. aegypti* was examined using the assays previously used for *An. gambiae*. As in *An. gambiae*, *Ae. aegypti Ir93a* mutants remained fully capable of initially responding to multiple host-associated cues (Figures 7C–D, Figures S5B and S5C). However, consistent with an impact on host detection, *AaIr93a* mutants showed diminished attraction to a human hand at later time points in the assay compared to controls (Figures 7E, Figure S5D, Dataset S1), a defect in sustained attraction reminiscent of that observed in *AgIr93a* mutants (Figures 6B and 6E). Blood feeding from collagen membrane feeders was also reduced in *AaIr93a* mutants, with ~30 to ~40% of mutant females consuming a blood meal compared to ~80% of control (Figure 7F; Figure S5E). Thus, *Ir93a*-dependent signaling contributes to host detection and blood feeding in both *Ae. aegypti* and *An. gambiae.*

AaIr93a mediates oviposition site seeking

Gravid *Ae. aegypti* females often lay their eggs in water-holding containers associated with human habitats, including discarded tires and buckets, a behavior thought to have contributed to their successful domestication and global spread [36,37,49]. As *Ae. aegypti* mosquitoes did not participate in the water-seeking assay used for *An. gambiae*, we tested

their ability to seek potential oviposition sites inside water-holding containers. ~70 gravid female mosquitoes (previously mated and 72h after blood feeding) were provided a choice of two containers, each lined with filter paper as an oviposition substrate: one ~75% full of water, the other dry (Figure 8A). A mesh with a central opening (~5 mm in diameter) covered each container, allowing water vapor escape and mosquito entry, while minimizing incidental contact between mosquito and oviposition site (Figure 8A). By 24 hours, wild type females had laid hundreds of eggs in the wet container (median ~370); in stark contrast, in the majority of assays, *AaIr93a* mutants laid none (Figures 8B–D). (No genotype laid eggs in the dry container.) Consistent with this egg laying defect reflecting a failure in seeking out the oviposition site, far fewer *AaIr93a* mutant than wild type females were observed within the wet container at assay end (Figure 8B; Figure S6A).

Importantly, the egg laying defect did not reflect an underlying failure of egg development. Control experiments revealed that the ovaries of gravid *AaIr93a* mutants contained no fewer mature oocytes than controls (Figure 8E, Figure S6B). Most importantly, when placed within an oviposition chamber (bypassing the need to seek an oviposition site), *AaIr93a* mutants and controls laid similar numbers of eggs (Figures 8F and 8G). Thus, the *AaIr93a* mutants are defective in oviposition site seeking, rather than in producing or laying eggs. Together, these data demonstrate that *AaIr93a*-dependent sensors are critical in helping gravid *Ae. aegypti* females locate water-filled containers for oviposition.

Discussion:

Here we show that *Ir93a*-dependent signaling in mosquitoes promotes behaviors related to blood meal acquisition and oviposition site location. Both these behaviors have central roles in the cycle of vector-borne disease. Blood feeding is essential for vector reproduction, as females require a blood meal to produce mature eggs [34]. Blood feeding is also essential for disease transmission: female mosquitoes acquire pathogens from infected hosts during blood feeding, and then transmit them to other hosts during subsequent blood meals [6]. These contributions make the rate of blood feeding a significant determinant of vector-borne disease levels [7]. In addition, oviposition is also critically linked to vector reproduction, as gravid females need to locate pools of water to support offspring development [34]. Thus, our findings reveal that *Ir93a*-dependent sensory signaling modulates behaviors that impact multiple aspects of vector reproduction and disease transmission. This *Ir93a*-dependence is shared between the malaria vector *An. gambiae* and the arbovirus vector *Ae. aegypti*, demonstrating that common molecular machinery supports these behaviors in members of both subfamilies of blood-feeding mosquitoes.

Ir93a acts in multiple subsets of mosquito sensory neurons

At the level of sensory transduction, we find that *Ir93a* mediates hygrosensation and thermosensation in the mosquito, acting in the mosquito's Cooling Cells, Dry Cells and Moist Cells. Work in multiple insect species indicates that IR-dependent sensory neurons commonly express multiple classes of IRs which together mediate sensory transduction [50–52]. Such combinations usually consist of one or more broadly expressed co-receptor IRs, as well as one or more stimulus-specific IR, the latter responsible for determining

sensory specificity. *Ir93a* is a co-receptor particularly active in insect hygrosensory and thermosensory neurons, where it operates alongside a second (more broadly expressed) co-receptor, *Ir25a* [23–25,32, 42]. In *Drosophila melanogaster*, each *Ir93a* function also involves a stimulus-specific IR: *Ir21a* in Cooling Cells [32], *Ir40a* in Dry Cells [23,25] and *Ir68a* in Moist Cells [24]. In mosquitoes, *Ir21a* mediates thermosensing [11], while the contributions of *Ir25a, Ir40a* and *Ir68a* to heat and humidity sensing remain to be examined. As *Ir93a* is also expressed in a subset of mosquito olfactory neurons, it could also function with additional stimulus-specific IRs.

Heat- and humidity-seeking relies on sensors previously implicated in insect homeostasis

Ir93a and its partners are conserved from crustaceans to insects [42,53,54], indicating they emerged ~250 million years before blood feeding (Figure 8H). Accordingly, they would have initially served other functions, potentially including thermoregulation and water balance as in contemporary *Drosophila* [23–26,32]. From an evolutionary perspective, this suggests that the evolution of mosquito hematophagy did not involve the generation of novel thermosensors and hygrosensors to detect the heat and humidity emitted by warm-bodied hosts. Rather, the evolution of mosquito hematophagy appears to have involved co-opting existing detectors of environmental stimuli important for organismal homeostasis.

It is also noteworthy that *Ir93a*, as well as *Ir21a*, *Ir25a*, *Ir40a* and *Ir68a*, emerged before the ancestors of modern insects colonized land (Figure 8H). Thus, heat- and humidity-sensing in vector mosquitoes involves a molecular toolkit that emerged in the Cambrian (or possibly Ediacaran) oceans (Figure 8H). The presence of orthologs of hygrosensory IRs in aquatic creatures is particularly striking, as hygrosensation is inherently terrestrial. However, *Ir93a*-dependent hygrosensors innervate poreless sensilla, suggesting they do not detect humidity directly, but via a humidity-dependent stimulus transmitted through the cuticle, such as force [22,55]. Crustacean orthologs of these insect IRs might therefore detect similar sensory stimuli produced by different external cues, for example, pressure at different water depths.

Although heat and humidity serve as host cues for many blood-feeding insects in addition to mosquitoes, including kissing bugs, tsetse flies, and stable flies [14,56–58], blood feeding arose independently in several of these lineages [33,59] (Figure 8H). Thus, while *Ir93a* and its partners are conserved across blood-feeding insects (Figure 8H), their contributions to host-seeking in other insect lineages would reflect evolutionary convergence. As insects possess multiple non-IR-dependent pathways for detecting physical cues (e.g., TRP channels) [60], it will be of interest to determine how broadly *Ir93a*-dependent signaling has been co-opted for host seeking across insect vectors.

Ir93a mediates attraction to potential egg laying sites

Our data also demonstrate that *Ir93a* plays a central role in helping gravid female mosquitoes seek high humidity associated with preferred egg laying sites. Most dramatic perhaps, given the importance of water bottles, discarded tires and other containers in *Ae. aegypti* reproduction [39], we show that *AaIr93a*-dependent sensors allow gravid *Ae.*

aegypti females to locate water-filled containers for oviposition. As liquid water generates humidity gradients, pools of water provide both diffusible (humidity) and contact (liquid water) cues that promote oviposition. Our data support a model in which gravid female mosquitoes respond to water's distinct phases using distinct sensory pathways. Specifically, *AaIr93a* drives attraction to potential oviposition sites by detecting water vapor, but is not required for oviposition once at the site. On the other hand, other sensors, including the previously described cation channel *ppk301*, regulate egg-laying decisions at later stages, upon contact with liquid water [37]. Less is known regarding *An. gambiae* oviposition, but the requirement for *AgIr93a* in water-seeking by gravid females (Figures 5B and 5C) is consistent with a similar role for this pathway in Anopheline mosquitoes. Ultimately, oviposition (like host seeking and blood feeding) involves multi-sensory integration, and it will be of interest to examine how mosquitoes combine the detection of humidity with other oviposition-regulating stimuli, including visual, olfactory and contact cues [36], to generate this behavior.

Limitations of this study

As *Ir93a* mediates sensory responses alongside several modality-specific IR partners, including *Ir21a*, *Ir40a,* and *Ir68a* in *Drosophila*, it will be important to further dissect the contributions to mosquito behaviors of individual subclasses of *Ir93a*-expressing neurons, particularly contributions to behaviors that involve responses to complex targets like human hosts. For example, *Ir93a* could potentially mediate responses not only to the heat and humidity humans produce, but additional unknown host cues. The study of modality-specific partners has already been informative for investigating *Ir93a*'s thermosensory role, as the examination of mosquitoes mutant for *Ir21a* implicated cooling-activated thermosensors as major drivers of heat-seeking in *An. gambiae* [11]. Studies of *Ir40a* and *Ir68a* mutants should be similarly useful in probing Dry Cell and Moist Cell function. In addition, while this present work focuses on the sensory periphery, how thermosensory and hygrosensory inputs are integrated with each other and with other sensory input in the brain remains an open question. This is particularly interesting given the multi-modal nature of mosquito host seeking [61], and should be facilitated by the tools developed here. Additionally, our behavioral studies are limited in being laboratory-based and designed to prevent biting of the host. As classic field studies on mosquito host seeking assigned paramount importance to humidity and temperature [62], it will be of interest to determine whether *Ir93a* mutants assayed under semi-field conditions behave similarly to those assayed using cages, remaining capable of host approach, but defective in maintaining short range interactions. It will also be important to determine how the loss of *Ir93a* impacts mosquitoes permitted to bite the host. While contact with human skin and blood provides additional mechanosensory and chemosensory cues, temperature and humidity stimulate probing [63,64], so *Ir93a*-mediated signaling could help promote and position the bite.

From an evolutionary perspective, the parallel functions of *Ir93a* in *An. gambiae* and *Ae. aegypti* are consistent with *Ir93a* mediating blood feeding in a common ancestral hematophage. However, studies in additional species are needed to test this view. Finally, as the mosquitoes studied here feed on mammals and birds, it will be of interest to examine

Ir93a function in mosquitoes that normally feed on animals whose thermal and possibly humidity cues are weak or absent, like amphibians [65].

Potential impacts of identifying the mosquito hygrosensors

In addition to basic insights into blood feeding and oviposition, the impact of *Ir93a* disruption on behaviors critical for reproduction and disease transmission raises the possibility of attempting to use these insights for practical purposes. In particular, the absence of close mammalian relatives of IRs could enhance their attractiveness as potential targets for control agents to disrupt blood feeding or oviposition. In fact, humidity sensing neurons have recently been proposed as targets for control agents [66]. However, initial efforts have focused on compounds that affect basiconic sensilla (based on prior literature [29]), rather than sensilla ampullacea. Identification of the *Ir93a*-dependent mosquito hygrosensors provides a new cellular and molecular focus for such approaches as well as new tools for assessing hygrosensory function. Such insights may be useful in helping develop approaches to disrupt blood feeding and oviposition by disease-spreading mosquitoes.

STAR Methods text:

Resource availability

Lead contact—Further information and requests for resources and reagents should be directed to and will be fulfilled by the lead contact, Paul Garrity (pgarrity@brandeis.edu)

Materials availability—All unique/stable reagents generated in this study are available from the Lead Contact without restriction.

Data and code availability

- Data: All data in this paper are available upon request from the lead contact.
- Code: The source code for the Calcium Imaging analysis is available as a text file at DOI: 10.7554/eLife.26654.010.
- Any additional information required to reanalyze the data reported in this paper is available from the lead contact upon request.

EXPERIMENTAL MODEL AND SUBJECT DETAILS

Mosquito rearing and maintenance—*Anopheles gambiae* (G3 strain [11]) and *Aedes aegypti* (LVP strain [71]) mosquitoes were grown in incubators (Percival Scientific) maintained at 27°C and 70–80% relative humidity with a 12-hour light/dark cycle. Larvae were raised in trays of deionized water and fed a mixture of powdered commercial fish foods (TetraMin flakes #77101 and TetraPond sticks #16467, Tetra Co., Melle, Germany) and Koi pellets (Kaytee, #100033588). Prior to eclosion, pupae were transferred to mesh cages (Bugdorm, MegaView Science Co., Ltd., Taiwan) where they remained as adults. Except where otherwise noted, adults were provided with constant access to water and 10% w/v glucose. A collagen membrane feeding system (Hemotek, ltd., Blackburn, UK) was used to provide warmed human blood (Research Blood Components, Watertown, MA) to adult female *Anopheles gambiae* and heparinized sheep blood (HemoStat Laboratories) to

adult female *Aedes aegypti*. Feeding procedures were approved and monitored by Brandeis Institutional Biosafety Committee (protocol #16015).

See Dataset S1 for a complete list of genotypes in the figures.

METHOD DETAILS

Measurement of humidity and temperature gradients—Temperature and humidity gradients associated with a human hand were measured under identical conditions to the host approach assay (see below). A human hand was placed on a 3mm high plastic mesh spacer situated on top of a mesh cage (Bugdorm, 17.5×17.5×17.5cm). Temperature and relative humidity levels were recorded at specific distances below the hand using a Sensirion EK-H4 sensor. Gradients were measured in triplicate from two independent volunteers in a randomized order. To calculate the steepness, gradients from each individual hand were calculated before being averaged. A Schlieren image of the environment surrounding a human hand was provided by Gary S. Settles, and obtained using described methods [13]. Schlieren imaging permits the visualization of refractive index variations within a transparent medium, such as those caused by variations in temperature and humidity.

Cloning—See Dataset S1 for an assembled list of oligonucleotides used in the study.

AgU6-IR93a gRNA_AgVasa-Cas9 plasmids: The coding sequence of *AgIR93a* (AGAP000256) was screened for Cas9 target sites devoid of predicted off-target activity using CHOPCHOP (https://chopchop.cbu.uib.no). One site in the putative pore and one site in the second transmembrane (TM2) region were chosen to create targeted knock-ins via homology directed repair. Complimentary oligonucleotides corresponding to the pore (5'-tgctGAACTGCTTCTGGTACATCTA-3' and 5'-aaacTAGATGTACCAGAAGCAGTTC-3') and TM2 (5'-tgctGAATCATCATCGGTACCTGG-3' and 5'-aaacCCAGGTACCGATGATGATTC-3') sites were annealed and cloned into the AgVasa-Cas9-sgRNA backbone vector[11] using Bsa1 restriction sites.

AaU6C-IR93a gRNA_AaExu-Cas9 plasmid: To generate a gRNA/Cas9 expression vector for Aedes aegypti, the AgVasa-Cas9-sgRNA backbone vector was modified to drive Cas9 expression from the AaExu promoter and sgRNA expression from the AaU6C promoter. The AaU6C promoter was amplified from U6c-T (addgene #117211; [72]) using 5'-GACATAAGACGTCCCGGGCCCATATGTCTTGC-3' and 5'-AAACGGTCTCTATCAATTAGCCTCATTCATCTTAG-3' and inserted using AatII/PmeI sites. The AaExu-Cas9-t2a-EGFP-p10 sequence from AAEL010097-Cas9 (addgene #100707; [73]) was then liberated by digestion with Asc1/AvrII sites and inserted using Asc1/Xba1 sites.

The coding sequence of AaIR93a (AAEL021659) was screened using CHOPCHOP. A site in exon 12 adjacent to TM1 was chosen to create a targeted knock-in (GCTCATAGAATGGGCTCAAGCGG). Complimentary oligonucleotides corresponding to the target site (5'-tgatGCTCATAGAATGGGCTCAAG-3' and 5'-

aaacCTTGAGCCCATTCTATGAGC-3') were annealed and cloned into the AaExu-Cas9-AaU6C-sgRNA backbone vector using Bsa1 restriction sites.

AgIR93a-T2A-QF2_attp_3xp3-XFP_attP plasmid: To generate an RFP-marked version of the previously characterized T2A-QF2_attp_3xp3-eYFP_attp donor backbone plasmid[11], the 3xp3-eYFP sequence was removed using Xba1/Mlu1 restriction sites and the 3xp3-RFP coding sequence from pDSAR [74]was amplified with gtagggtcgccgacatgacacaaggggtttctagaCGGTTCCCACAATGGTTAATTCG and cgacatgacacaaggggttctcgaGCCGTACCGTACGCGTATCGATAAGCTTTAAGATACATTGA before being inserted using SLiCE cloning [75].

To created targeted insertions in *Anopheles*, homology arms consisting of ~2kb immediately upstream and downstream of Cas9 cutsites were cloned into eYFP and RFP marked donor backbone plasmids using EcoRV/BamHI restriction sites for 5' homology arms and Asc1/Spe1 for the 3' homology arms. Homology arms were amplified from genomic DNA using the following PCR primer pairs:

AgIR93a pore-5HDR-fwd CCTGATCAACGAGGGTGAC

AgIR93a pore-5HDR-rev cgataccaGGATCCTATGTACCAGAAGCAGTTGTTCACC

AgIR93a pore-3HDR-fwd gtagcgaGGCGCGCCCTATGGTGCGCTACTGCAGC

AgIR93a pore-3HDR-rev TCGACactagtGGTTCATATGAGCGCTTTGG

AgIR93a TM2–5HDR-fwd CAGATATCGGACGAGGAGTG

AgIR93a TM2–5HDR-rev cgataccaGGATCCGGTACCGATGATGATTCGTCC

AgIR93a TM2–3HDR-fwd tagcaggcgcgccaTGGTGGTTGGGTATGTGCTG

AgIR93a TM2–3HDR-rev tcgacactagtGGTTCATATGAGCGCTTTGG

AaIR93a-T2A-QF2_attp_3xp3-XFP_attP plasmid: To create targeted insertions in *Aedes aegypti*, homology arms consisting of ~2kb immediately upstream and downstream of Cas9 cut sites were cloned into eYFP and RFP marked donor backbone plasmids using EcoRI/EcoRV restriction sites for 5' homology arms and Asc1/Spe1 for the 3' homology arms. Homology arms were amplified from genomic DNA using the following PCR primer pairs:

AaIR93a-5HDR-fwd aagtcaGAATTCGTTAGATCGGGACATTATCGCC

AaIR93a-5HDR-rev tAAGCGGTTAACGACGTACAGAAACGGTCCC

AaIR93a-3HDR-fwd atgcaaggcgcgccGAGCCCATTCTATGAGCACC

AaIR93a-3HDR-rev acgaatactagttCACCATCGTGACCTTCCCTTG

Generation of transgenic mosquito strains—*Anopheles coluzzii* QUAS-GCaMP6f [47] and QUAS-*m*CD8:GFP [45] strains were generously provided by Chris Potter. These strains

were crossed to *G3* for a minimum of five generations before being used in our experiments. *Aedes aegypti* QUAS-GCaMP7s [48] and QUAS-mCD8:GFP [37] were generously provided by Lindy McBride. *Anopheles gambiae Ir21a*$^{+7bp}$ and *Ir21a*^{eYFP} strains were previously described [11]. Generation of IR93a knock-in lines was accomplished using previously described methods[11]. Plasmids were prepared for injection using ZymoPURE II endotoxin-free midiprep kit (Zymo Research Corp, Irvine, CA). A mixture of Cas9/sgRNA plasmid (300ng/μl) and both color donor plasmids (150 ng/μl RFP and 150 ng/μl eYFP) was diluted in water for injection. Freshly laid embryos were aligned against wet nitrocellulose paper and injected near the posterior pole using beveled aluminosilicate needles and a PLI-100 picoinjector (Harvard Apparatus). Surviving injected individuals were crossed to wildtype stock and their F1 progeny were screened for RFP and eYFP fluorescence. Knock-in animals were further outcrossed to wildtype for a minimum of 5 generations.

To verify the correct insertion in *Anopheles*, animals were genotyped using a mix of three PCR primers (Universal forward primer 5'-CCATCCTATGTGCGATCAACAA-3', WT Rev 5'-GTACTTCGGTTCGGTCGAGTC-3' and IR93a Rev 5'-CCGTATTGGCCACGTGTCC-3'). PCR products were run on an agarose gel where WT and mutant alleles could be clearly distinguished based on size (586 bp for WT, 261bp for IR93a^{pore}, and 412 bp for IR93a^{TM2}).

To verify the correct insertion in *Aedes*, animals were genotyped using a mix of three PCR primers (Universal forward primer 5'-GACGCCTATCAGCATTCAAAC-3', WT Rev 5'-CGTCTACTAGAGTGTACATCTATTCTTACC-3' and IR93a Rev 5'-CCGTATTGGCCACGTGTCC-3') giving bands of 409bp for WT and 461bp for IR93a knock-in. PCR products were further verified by Sanger sequencing.

Single Sensillum Electrophysiology—Extracellular electrophysiological recordings from single antennal sensilla were performed as previously described[11]. Female mosquitoes (1–4 days old) were secured to glass slides with double sided tape and the antennae were flattened with human hair. A glass reference electrode was inserted into the eye and a recording electrode (filled with 130mM NaCl, 5mM KCl, 2mM $MgCl_2$, 2mM$CaCl_2$, 36mM D-sucrose, 5mM HEPES, pH 7.3) was inserted into one of the coeloconic sensilla found at the most distal tip of the 13th antennal segment. Thermal stimuli were delivered via two alternate streams of dry air passing over the antennae. Temperatures of the air streams were calibrated to 25°C and 30°C by initially passing them through a common tube submerged in a warm water bath after which the streams were split and the warmer airstream was passed through insulated tubing further heated with a resistor (Emron E5CSV). Temperature at the antennae was recorded using an IT23-thermocouple (Physitemp) and a Fluke 80TK thermocouple module. Electrical signals detected in the sensilla were amplified using a TasteProbe DTP-02 (Syntech) and digitized with PowerLab 8/30. Data was band-pass filtered (100Hz-3000Hz) and acquired at 20k/s with LabChart 7 (ADInstruments, RRID:SCR_017551). Spike thresholds were calculated by selecting the minimum interpeak value from spike amplitude histograms in Lab Chart 7. Spike rates were calculated as weighted average of Instantaneous Spike Frequencies across a 1 sec triangular window centered at the indicated time. Different time windows after onset were used to calculate

average cooling and heating responses as the rise in weighted average spike frequency upon cooling was faster and sharper than its drop upon warming.

Imaging and immunohistochemistry—To image CD8:GFP driven by IR93a, freshly dissected antennae of female mosquitoes were mounted in 80% glycerol/20% PBS and immediately imaged on an LSM 880 laser scanning confocal microscope (Zeiss). Immunostaining of cryosectioned mosquito antennae was performed as described[11]. Isolated mosquito heads (Genotype: AgIR93a^{pore}-T2A-QF2/+; QUAS-CD8:GFP/+) were fixed for 30 min with ice cold 4% paraformaldehyde in PBS-T. Fixative was removed by washing with PBS before heads were cryoprotected overnight in 25% sucrose. After cryoprotection, antennae were dissected from heads and mounted in OCT compound (Tissue-Tek). Sections (14–18 μm) were dried to slides for 30 min before fixing with 4% paraformaldehyde for 15 min at room temperature. Fixative was removed by washing with PBS-T before blocking with 10% normal goat serum in PBS-T for 1 hour at room temperature. Slides were then incubated with primary antibody (chicken anti-GFP, GFP-1010, Aves Lab, RRID:AB_2307313) diluted 1:1000 in 10% normal goat serum in PBS-T for 48 h at 4 C. Slides were washed 6 times for 20 minutes and incubated in secondary antibody (Alexa Fluor 488 goat anti-chicken-488, #A11039, Invitrogen, RRID: AB_2534096) diluted 1:200 in 10% normal goat serum for 3 hours in the dark at room temperature. Slides were washed 6 times for 20 min in PBS-T and mounted in Vectashield with DAPI (Vector Laboratories).

Whole-mount immunohistochemistry was adapted from [45]. Female mosquito heads were removed and digested for 1.5 hours at 37°C with 5U/mL chitinase (Sigma C6137) and 100U/mL chymotrypsin (Sigma CHY5S) resuspended in HEPES larval buffer (119mM NaCl, 48 mM KCl, 2mM $CaCl_2$, 2mM $MgCl_2$, 25mM HEPES, pH 7.5). Heads were quickly washed with ZnFa fixative (0.25% ZnCl2, 135mM NaCl, 1.2% sucrose, 0.03% Triton X-100, 2% PFA) before fixing for 24 hours at room temperature. After fixation, antennae were dissected in fresh HBS (150mM NaCl, 5mM KCl, 25mM sucrose, 10mM HEPES, 5mM CaCl2, 0.03% Triton X-100) then dehydrated for 1 hour in 80% methanol/20% DMSO. Antennae were then washed with 0.1M Tris pH 7.4, 0.03% Triton X-100 prior to blocking overnight at 4°C (1X PBS, 1% DMSO, 5% normal goat serum, 0.03% Triton X-100). Primary antibodies (mouse anti-*Apocrypta bakeri* Orco monoclonal antibody #15B2 [76] (1:50 dilution) and chicken anti-GFP, GFP-1010, Aves Lab (1:500 dilution, RRID: AB_2307313)) were diluted in blocking buffer and incubated with the tissue for 72 hours at 4°C. Primary antibodies were washed 5 times with 0.03% PBS-TritonX-100, 1% DMSO for 30 minutes followed by an overnight was at 4°C. The next day, antennae were incubated with secondary antibodies diluted in blocking buffer for 72 hours at 4°C (Cy5 goat anti-mouse (1:200, RRID: AB_2534033) and Alexa Flour488 goat anti-chicken (1:200, RRID: AB_2534096)). Secondary antibodies were removed with the wash protocol used for primary antibodies. Antennae were then washed with PBS and mounted with Vectashield with DAPI.

Fluorescent in-situ hybridization—Hybridization chain reaction (HCR) based fluorescent in-situ hybridization (FISH) was used detect IR93a mRNA in whole mount preparations of *Aedes aegypti* and *Anopheles gambiae* antennae as previously described

[77,78]. Probe sets, amplifiers and HCR RNA-FISH buffers were procured from Molecular Instruments (molecularinstruments.com/) and described in Dataset S1. The following probe sets and HCR-amplifiers were used in this study:

Target gene	Probe lot number	Amplifier	Fluorophore
Aedes aegypti Ir93a (AAEL021659)	PRD478	B4	Alexa 647
Aedes aegypti Orco (AAEL005776)	PRC 276	B1	Alexa 546
Anopheles gambiae Ir93a (AAEL021659)	PRK 975	B4	Alexa 647

Female mosquitoes aged between 5–8-days old were briefly anesthetized on ice and their heads were dissected out carefully, leaving both antennae intact. The heads were then digested in a Chitinase Chymotrypsin (CCD) buffer (composition: 5 U/mL chitinase, 100 U/mL alpha-chymotrypsin, 2% DMSO in HEPES Larval Buffer: 119 mM NaCl, 48 mM KCl, 2 mM $CaCl_2$, 2 mM $MgCl_2$, 25 mM HEPES) at 37°C in a rotating hybridization oven for 30 minutes. The heads were then fixed in 4% PFA (composition: 4% PFA in 1X PBS, 0.03% Triton X-100) on a nutator at 4°C for 24 hours. Following PFA fixation, the heads were subject to four, 5-minute washes in 0.1% PBS-Tween on ice. Whole antennae were then removed and collected in an Eppendorf tube containing 0.1% PBS-Tween on ice. The antennae were dehydrated by sequentially washing in a graded methanol series composed of 25%, 50%, 75% MeOH dissolved in 0.1% PBS-Tween and twice in 100% MeOH for 10 minutes each on a nutator at 4°C. The antennae were then incubated in 100% MeOH overnight and re-dehydrated the next day with sequential 10 minutes washes in a graded methanol series containing 75%, 50%, 25% MeOH in 0.1% PBS-Tween, and finally twice in 0.1% PBS-Tween-20 alone. The antennae were next digested in 20 pg/mL Proteinase-K solution in 0.1% PBS-Tween for 30 minutes at RT. After washing two times in 0.1% PBS-Tween for 10 minutes each at RT, tissue was post-fixed in 4% PFA for 20 minutes at RT. Following three 15-minute washes in 0.1% PBS-Tween at RT, antennae were incubated in probe hybridization buffer for 30 minutes at 37°C. A probe solution was prepared by dissolving 8 pmol of each probe in 500ul probe hybridization buffer at 37°C. Antennae were incubated in the probe solution at 37°C while rotating in a hybridization oven for two nights. Next, the antennae were washed five times for 10 minutes each in probe wash buffer at 37°C in a hybridization oven. Antennae were further washed in 5X SSCT twice for 5 min at RT and incubated in amplification buffer for 10 min at RT. 18 pmol each of hairpins h1 and h2 were snap cooled and added to 100 µl amplification buffer at RT. Antennae were incubated in hairpin solution for two nights while incubating overnight on a nutator at RT and were shielded from light exposure. Tissue was washed in 5X SSCT five times at RT and mounted in Slow Fade gold on glass slides for imaging. Images of the 1st, $2^{nd,}$ and 13^{th} antennal flagellomeres were acquired on a Zeiss LSM 880 confocal microscope, using a 40X (1.4 N.A.) oil-immersion objective at 512 × 512-pixel resolution.

Calcium imaging—Transcuticular calcium imaging was performed based on a previous study [47]. Animals were anesthetized on ice and their wings and legs were removed. Antennae were affixed to a glass slide with double sided tape and human hair. Images were acquired from the medioventral aspect of the second flagellomere for hygrosensory

stimuli and the distal tip of the thirteenth flagellomere for thermosensory stimuli using an Olympus BX51WI microscope fitted with an Olympus SLMPlan 50x/0.45 objective and a Hamamatsu Orca-R2 camera recording at 4 frames/sec for hygrosensory recordings and 10 frames/sec for thermosensory recordings.

Hygrosensory stimuli were applied as described previously [23]. A dry airstream (500ml/min) was connected to a solenoid valve that split the stream into two paths. The dry stream (~7% RH) was passed through an empty glass flask while the humid airstream (~90% RH) was bubbled through a flask filled with distilled water. During imaging, one airstream flowed for the first 5s before switching to the other stream for 10s after which it returned to the original stimulus for 5s. The starting condition (dry or humid) was alternated between individuals. Recordings were processed in Fiji (RRID:SCR_002285) using Stackreg [79] to correct for movement. Baselines (F_0) were calculated by taking the average of frames 7–24 preceding the first change in humidity. Moist and dry responses were quantified by taking the average of 10 consecutive frames where responses were found to be maximal across samples (frames 41–50 for DWD paradigm and frames 46–55 for the WDW paradigm).

Thermal stimuli were delivered via two alternate streams of dry air passing over the antennae. Temperatures of the air streams were calibrated by passing the tubing through a water bath after which the hot airstream was passed through insulated tubing further heated with three resistors (Emron E5CSV). Temperature at the antennae was recorded using an IT23-thermocouple (Physitemp). During imaging, one airstream flowed for the first 15s before switching to the other stream for 30s after which it returned to the original stimulus for 15s. The starting condition (warmer or cooler) was alternated between individuals. Recordings were processed in Fiji (RRID:SCR_002285) using Stackreg [79] to correct for movement. Baselines (F_0) were calculated by taking the average of 5s to 1s preceding the first change in temperature. Responses were quantified by taking the average ΔF/Fo from 15 to 25 sec after this temperature shift.

Heat seeking Assay—Heat seeking assays were performed as previously described[11]. A custom white plexiglass box (28×40×16cm) with transparent front viewing panel was used as the behavioral chamber. Two temperature-controlled Peltier elements (Custom Thermoelectric, LLC, Bishopville, MD) were mounted on the rear wall of the box, covered by white printer paper to match the surroundings. Likewise, a white gas diffusion pad was mounted on the ceiling to allow for introduction of CO_2. The night before an experiment, 46–50 mated female mosquitoes (7–14 days old) were anesthetized on ice and placed into the heat seeking box. Animals were starved overnight with access to water-saturated cotton balls. Mosquitoes were maintained on an inverted light/dark cycle such that the lights were on during the overnight acclimation period and switched off 1 hour before the start of the assay. Environmental conditions in the behavior room were 25°C with a relative humidity of 70%. The experiments began when a randomly assigned Peltier unit was heated to 37°C while the other was set to 26°C. After 1-minute, a 20-second pulse of 4% CO_2 (4% CO_2, 21% O_2, balance N_2) was introduced through the diffuser pad. Mosquito activity was recorded using a front-mounted infrared camera (B00UMX3HEG) recording at 30 images/second. The number of animals on each Peltier was manually counted at 5 second intervals before being normalized for the CO_2 takeoff response of each trial. CO_2 takeoff

was assessed by analyzing the individuals in view just prior to CO_2 pulse and quantifying the percentage that took flight after the pulse. A heat-seeking index was then defined as the percent of mosquitoes landed on a Peltier divided by the percent CO_2 takeoff of the trial. A single trial of G3 mosquitoes failed to activate in response to CO_2 application and was therefore excluded from analysis.

Host Approach Assay—Host approach assays were performed as previously described[11]. Female mosquitoes (4–10 days old) were separated from males and housed in cages of 41–76 animals (Bugdorm, 17.5×17.5×17.5cm). Mosquitoes were starved overnight and the next day the cages were removed from the incubator to acclimate to testing room conditions for 2 hours without water. To begin the experiment, 5 short human breaths were blown into the cage to activate host-seeking behaviors. A 3mm high plastic mesh spacer was placed on the roof of the cage and the hand of a human volunteer was placed on the spacer such that the mosquitoes could approach the hand but could not make direct contact with their proboscis or other appendages. The same female volunteer was used for all *Anopheles* assays and a different female volunteer was used for all *Aedes* assays. An iPhone XR camera was used to record the entire 5-minute period the hand was presented to the animals, followed by an additional minute after the hand was removed. The number of animals accumulated under the hand was quantified at 5 second intervals for the duration of the assay and divided by the total number of animals in the cage to give the percentage approaching the host. Individuals were categorized as flying, resting, or probing by selecting a specific frame and manually assigning a category to each individual based on their movements seen in the prior and subsequent frames.

Blood feeding Assay—Blood feeding assays were performed as previously described[11]. 47–76 mated female mosquitoes (5–15 days old) were sexed on ice and starved overnight. The next day, cages were removed from the incubator to acclimate to testing room conditions (21–24°C, ~50% RH) for ≥1 hr. After acclimating, warmed blood was provided through the mesh roof of the cage via a collagen membrane feeding system (Hemotek, ltd., Blackburn, UK). *Anopheles* experiments were performed using human blood, while *Aedes* experiments were performed using heparinized sheep blood supplemented with 1mM ATP. Animals were allowed to feed for 20 minutes, after which they were collected on ice and squished onto white filter paper to check for evidence of a blood meal. Overall cage health was assessed by performing a host approach assay on the cages >1hr before blood feeding.

Humidity-seeking Assay—For humidity seeking, newly eclosed female *Anopheles* mosquitoes were housed together for 4–13 days. For trials with non-blood-fed females, animals were separated into cages of 25–73 females. For trials of gravid females, animals were offered warmed human blood and engorged individuals were separated on ice into cages of 27–66 females for testing 48 hours later. All animals were starved overnight before testing. Two hours before the start of experiments, water was removed and cages were allowed to acclimate to testing room conditions (22–24°C and 25–51% RH). Immediately following the acclimation period, animals were machine aspirated and released into the experimental chamber by gentle shaking to avoid the use of human breath. The experimental setup consisted of a polypropylene cage (30×30×30cm, BugDorm-1) with two rectangular

8-well dishes (12.8×8.55×1.5cm) situated in the middle of the floor. One tray was empty and the other was half filled with water. Both trays were covered with custom 3D-printed mesh covers that allow water vapor to escape but prevent animals from being able to contact the liquid with their proboscis. Once released into the testing chamber, a camera (B00UMX3HEG) situated above the cage recorded the animals' movements throughout the 1hr assay. The number of animals contacting the mesh lids of each tray was counted at 1 min intervals. To verify the health and responsiveness of the non-gravid females, human breath was applied to the cage at the conclusion of the experiment and the number of animals that took flight during the subsequent 2 min interval was quantified.

Oviposition Assays—Mixed cages of newly eclosed male and female mosquitoes were maintained for 6–12 days before being blood-fed with warmed heparinized sheep blood supplemented with 1mM ATP. Fully engorged females were sorted on ice and split into cages of 70 individuals (Bugdorm, 30×30×30cm). Animals were housed for 72 hours with access to water and sugar solution. After 72 hours, food and water were removed and replaced with two cylindrical glass egg-laying dishes (7cm diameter, 5cm tall) lined with white filter paper and covered with tightly stretched mesh with a single entrance hole (0.5cm diameter) cut into it. One egg dish was filled ~75% full with water while one was left empty. After 24 hours, covered egg dishes were removed, trapped animals were counted, and the remaining animals were given access to sugar and an uncovered water-filled egg dish for 72 hours. The number of eggs laid in the initial covered dish and the subsequent uncovered dish were counted under a dissection microscope. To quantify the number of mature oocytes per female, animals were dissected in PBS 72 hours after blood feeding. The number of oocytes per ovary was quantified using a dissection microscope. To quantify egg-laying behavior when forced into close proximity with water, engorged females were separated on ice into individual filter paper-lined oviposition chambers (3oz Dixie® brand cups) covered with mesh. Animals were provided water and sugar using saturated cotton. Water was added to the oviposition cups 72 hours after blood feeding and the number of eggs laid was counted 24 hours later.

Quantification and statistical analysis—In all cases, n refers to independent biological replicates involving different animals or groups of animals. Shapiro-Wilk tests were used to assess the normality of all data sets ($p \leq 0.05$ rejected normal distribution). Parametric tests were performed on groups with normally distributed data. For single comparisons, a two-sided unpaired t-test was used. ANOVA with Tukey HSD post doc test was used for multiple comparisons (JMP11, SAS, RRID:SCR_014242). If any data set did not exhibit a normal distribution, non-parametric tests were performed. Nonparametric tests consisted of either Wilcoxon (for single comparisons) or Kruskal-Wallis followed by a Steel-Dwass or Steel with control post hoc test for multiple comparisons (JMP11, SAS, RRID:SCR_014242). In box plots, the box represents inter-quartile range (IQR), midline represents median, and whiskers extend to the lowest or highest data point that falls within 1.5 times the IQR from the box edges.

The Shapiro-Wilk test and t-test/ANOVA/Tukey HSD or Wilcoxon/Kruskal-Wallis/Steel with control/Steel-Dwass values obtained are listed below:

For the Moist Cell responses in Figure 4: Response to moist air: +/*AgIr93a*^{pore}: W=0.947, p = 0.702; *AgIr93a*^{pore} : W = 0.956, p = 0.768; t-test, p < 0.0001. Response to dry air: +/*AgIr93a*^{pore}: W=0.970, p = 0.897; *AgIr93a*^{pore} : W = 0.884, p = 0.208; t-test, p = 0.006.

For the Dry Cell responses in Figure 4: Response to moist air: +/*AgIr93a*^{pore}: W=0.947, p = 0.704; *AgIr93a*^{pore} : W= 0.882, p = 0.198; t-test, p = 0.0002. Response to dry air: +/*AgIr93a*^{pore}: W= 0.920, p = 0.471; *AgIr93a*^{pore} : W = 0.695, p = 0.002; Wilcoxon: H = 10.54, p = 0.001.

For the 30°C to 25°C cooling responses in Figure 4: *wt*: W= 0.742, p = 0.03; *AgIr93a*^{TM2} : W=0.704, p = 0.01; Wilcoxon: H = 6.82, df = 1, p = 0.009.

For the 25°C to 30°C warming responses in Figure 4: *wt*: W= 0.880, p = 0.31; *AgIr93a*^{TM2} : W=0.930, p = 0.59; t-test, p = 0.0026.

Humidity-seeking assays in Figure 5: Not gravid females: For (% wet, average from 51 to 60 min) – (% dry, average from 51 to 60 min) : *wt*: W = 0.885, p = 0.083; *AgIr93a*^{pore} : W = 0.892, p = 0.284; *AgIr93a*^{TM2} : W = 0.794, p = 0.012; *AgIr21a*^{EGFP}: W = 0.765, p = 0.0408; Kruskal-Wallis: H = 22.08, df = 3, p < 0.0001. Steel with Control (vs wild type): wt vs. *AgIr93a*^{pore}, p = 0.0059; wt vs. *AgIr93a*^{TM2}, p = 0.0005, wt vs. *AgIr21a*^{EGFP}, p = 0.850. Gravid females: *wt*: W = 0.99, p = 1; *AgIr93a*^{TM2} : W = 0.95, p = 0.88. t-test: p = 0.009.

For CO2 takeoff at 60 min in response to breath in Figure S2: *wt*: W = 0.861, p = 0.040; *AgIr93a*^{pore} : W = 0.846, p = 0.112; *AgIr93a*^{TM2} : W = 0.962, p = 0.810; *AgIr21a*^{EGFP}: W = 0.975, p = 0.908; Kruskal-Wallis: H = 5.527, df = 3, p = 0.137.

For heat-seeking indexes in Figure 5: *wt*: W= 0.996, p = .999; *AgIr93a*^{pore} : W=0.754, p = 0.009; *AgIr93a*$^{pore/TM2}$: W=0.827, p =0.042. Kruskal-Wallis Test: H = 14.55, df = 2, p=0.0007. Steel-Dwass test (p-value of each pairwise comparison): *wt* vs. *AgIr93a*^{pore}, p = 0.0061; *wt* vs. *AgIr93a*$^{pore/TM2}$, p = 0.0029; *AgIr93a*^{pore} vs. *AgIr93a*$^{pore/TM2}$, p = 0.5014.

For CO_2 take-off in heat-seeking assays in Figure S2: *wt*: W= 0.888, p = .263; *AgIr93a*^{pore} : W=0.882, p = 0.199; *AgIr93a*$^{pore/TM2}$: W=0.838, p =0.055. ANOVA [F(2,21) = 3.00, p =0.07].

For hand-seeking in Figure 6D: Accumulation beneath hand at 60 sec: *wt* : W = 0.955, p = 0.724; *AgIr93a*^{pore}: W = 0.734, p = 0.014; *AgIr93a*^{TM2}: W = 0.904, p = 0.468; Kruskal-Wallis, H = 1.61, df = 2, p=0.45.

For hand-seeking in Figure 6E: Accumulation beneath hand (average from 240 to 300 sec): *wt* : W = 0.955, p = 0.724; *AgIr93a*^{pore}: W = 0.924, p = 0.503; *AgIr93a*^{TM2}: W = 0.968, p = 0.880; ANOVA [F(2,20) = 13.59, p =0.0002]. Tukey HSD alpha = 0.01.

For hand-seeking in Figure 6F: Percentage in flight at 240s: *wt* : W = 0.862, p = 0.080; *AgIr93a*^{pore}: W = 0.953, p = 0.753; *AgIr93a*^{TM2}: W = 0.949, p = 0.729; ANOVA [F(2,20) = 8.84, p =0.0018]. Tukey HSD alpha = 0.05.

For blood feeding in Figure 6H: *wt* : W = 0.918, p = 0.304; *AgIr21a*$^{+7bp}$: W = 0.923, p = 0.419; *AgIr93a*^{pore}: W = 0.688, p = 0.0003; *AgIr93a*^{TM2}: W = 0.846, p = 0.183; Kruskal-Wallis, H = 23.97, df = 3, p<0.0001. Steel-Dwass test (p-value of each pairwise comparison): *wt* vs. *AgIr21a*$^{+7bp}$, p = 0.665; *wt* vs. *AgIr93a*^{pore}, p = 0.0013; *wt* vs. *AgIr93a*^{TM2}, p = 0.0119; *AgIr21a*$^{+7bp}$ vs. *AgIr93a*^{pore}, p = 0.0060; *AgIr21a*$^{+7bp}$ vs. *AgIr93a*^{TM2}, p = 0.0175; *AgIr93a*^{pore} vs. *AgIr93a*^{TM2}, p = 0.5249.

For blood feeding in Figure S3: 37°C collagen, W = 0.918, p = 0.310; 26°C collagen, W = 0.783, p = 0.125; 37°C parafilm, W = 0.920, p = 0.742; 26°C collagen, not applicable. ANOVA [F(3,19 = 21.25, p <0.001]. Tukey HSD alpha = 0.05.

For hand-seeking in Figure 7D: Accumulation beneath hand at 60 sec: *wt* : W = 0.951, p = 0.733; *AaIr93a*^{EYFP}: W = 0.873, p = 0.273; *AaIr93a*$^{EYFP/RFP}$: W = 0.953, p = 0.892; ANOVA [F(2,19) = 0.12, p =0.89].

For hand-seeking in Figure 7E: Accumulation beneath hand (average from 270 to 300 sec): *wt* : W = 0.914, p = 0.32; *AaIr93a*^{EYFP}: W = 0.949, p = 0.865; *AaIr93a*$^{EYFP/RFP}$: W = 0.985, p = 1.00; ANOVA [F(2,19) = 5.283, p =0.015]. Tukey HSD alpha = 0.05.

For blood feeding in Figure 7F: *wt* : W = 0.904, p = 0.176; *AaIr93a*^{EYFP}: W = 0.919, p = 0.592; *AaIr93a*$^{EYFP/RFP}$: W = 0.852, p = 0.186. ANOVA [F(2,21) = 59.44, p <0.0001]. Tukey HSD alpha = 0.01.

For the cooling response in Figure S5: control (*AaIr93a*^{RFP} or ^{EYFP}/+): W = 0.9; p = 0.31; *AaIr93a*$^{EYFP/RFP}$: W = 0.983; p = 1.00. t-test = 0.00038.

For the warming response in Figure S5: control (*AaIr93a*^{RFP} or ^{EYFP}/+): W = 0.912; p = 0.35; *AaIr93a*$^{EYFP/RFP}$: W = 0.854; p = 0.19. t-test = 0.00213.

For hand-seeking in Figure S5C: Accumulation beneath hand at 60 sec: *wt* : W = 0.951, p = 0.733; *AaIr93a*^{RFP}: W = 0.947, p = 0.88; *AaIr93a*^{EYFP}: W = 0.873, p = 0.273; *AaIr93a*$^{EYFP/RFP}$: W = 0.953, p = 0.892; ANOVA [F(3, 28) = 4.01, p =0.017]. Tukey HSD alpha = 0.05.

For hand-seeking in Figure S5D: Accumulation beneath hand (average from 270 to 300 sec): *wt* : W = 0.914, p = 0.32; *AaIr93a*^{RFP}: W = 0.926, p = 0.43; *AaIr93a*^{EYFP}: W = 0.949, p = 0.865; *AaIr93a*$^{EYFP/RFP}$: W = 0.985, p = 1.00; ANOVA [F(3, 28) = 10.84, p < 0.001]. Tukey HSD alpha = 0.05.

For blood feeding in Figure S5E: *wt* : W = 0.904, p = 0.176; *AaIr93a*^{RFP}: W = 0.872, p = 0.13; *AaIr93a*^{EYFP}: W = 0.919, p = 0.592; *AaIr93a*$^{EYFP/RFP}$: W = 0.852, p = 0.186. ANOVA [F(3, 29) = 30.23, p <0.0001]. Tukey HSD alpha = 0.01.

For egg laying assay in Figure 8D: *wt* : W = 0.88, p = 0.21; *AaIr93a*^{RFP}: W = 0.6, p = 0.002; *AaIr93a*^{EYFP}: W = NA, p = NA. Kruskal-Wallis, H = 17.16, df = 2, p = 0.0002. Steel-Dwass test (p-value of each pairwise comparison among wet containers): *wt* vs. *AgIr93a*^{EYFP}, p = 0.001; *wt* vs. *AgIr93a*^{RFP}, p = 0.01; *AgIr93a*^{EYFP} vs. *AgIr93a*^{RFP}, p = 0.31.

For egg production in Figure 8E: *wt* : W = 0.958, p = 0.658; *AaIr93a*^{RFP}: W = 0.857, p = 0.044; *AaIr93a*^{EYFP}: W = 0.915, p = 0.187; Kruskal-Wallis, H = 11.98, df = 2, p=0.0025. Steel-Dwass test (p-value of each pairwise comparison): *wt* vs. *AgIr93a*^{EYFP}, p = 0.52; *wt* vs. *AgIr93a*^{RFP}, p = 0.0055; *AgIr93a*^{EYFP} vs. *AgIr93a*^{RFP}, p = 0.02.

For egg laying assay in Figure 8G: *wt* : W = 0.94, p = 0.27; *AaIr93a*^{RFP}: W = 0.926, p = 0.129; *AaIr93a*^{EYFP}: W = 0.862, p = 0.009. Kruskal-Wallis, H = 3.43, df = 2, p = 0.18.

For females in Figure S6A: *wt* : W = 0.9, p = 0.32; *AaIr93a*^{RFP}: W = 0.58, p = 0.0013; *AaIr93a*^{EYFP}: W = 0.42, p = 0.00007. Kruskal-Wallis, H = 15.57, df = 2, p = 0.0004. Steel-Dwass test (p-value of each pairwise comparison among wet containers): *wt* vs. *AgIr93a*^{EYFP}, p = 0.002; *wt* vs. *AgIr93a*^{RFP}, p = 0.0127; *AgIr93a*^{EYFP} vs. *AgIr93a*^{RFP}, p = 0.74.

Supplementary Material

Refer to Web version on PubMed Central for supplementary material.

Acknowledgments:

We thank F. Catteruccia, C. McBride and C. Potter for mosquito strains and advice, G. Settles for Schlieren image, S. McIver for discussions, K. Menuz, D. Task and C.Y. Su for protocols, V. Ruta for anti-Orco antisera, C. Zhu for assistance with husbandry and gradient measurements, A. Daniels for assistance with cloning, and L. Huang, E. Marder, S. McIver, M. Rosbash and members of the Garrity lab for comments on the manuscript. Funding was provided by National Institute of Allergy and Infectious Diseases grants R01 AI122802 (to P.A.G.), R01 AI157194 (P.A.G.), R21 AI140018 (P.A.G.) and F31 AI133945 (C.G.), National Science Foundation grant IOS 1557781 (P.A.G.), National Institute of Neurological Disorders and Stroke grant 2T32NS007292–31 (W.J.L.) and Charles A. King Trust Postdoctoral Research Fellowship, Bank of America, N.A., Co-Trustees (W.J.L.).

REFERENCES:

1. WHO (2014). World Health Organization: A global brief on vector-borne diseases. WHO/DCO/WHD/2014.1.
2. Clements AN (1999). The Biology of Mosquitoes: Sensory Reception and Behaviour (CABI Publishing).
3. da Silva AF, Machado LC, de Paula MB, da Silva Pessoa Vieira CJ, de Morais Bronzoni RV, de Melo Santos MAV, and Wallau GL. (2020). Culicidae evolutionary history focusing on the Culicinae subfamily based on mitochondrial phylogenomics. Sci Rep 10, 18823. 10.1038/s41598-020-74883-3. [PubMed: 33139764]
4. Powell JR (2018). Mosquito-Borne Human Viral Diseases: Why Aedes aegypti? Am J Trop Med Hyg 98, 1563–1565. 10.4269/ajtmh.17-0866. [PubMed: 29557341]
5. Clements AN (1999). The Biology of Mosquitoes: Development, Nutrition and Reproduction (CABI Publishing).
6. Clements AN (2012). The Biology of Mosquitoes: Transmission of viruses and interactions with bacteria (CABI Publishing).
7. Brady OJ, Godfray HC, Tatem AJ, Gething PW, Cohen JM, McKenzie FE, Perkins TA, Reiner RC Jr., Tusting LS, Sinka ME, et al. (2016). Vectorial capacity and vector control: reconsidering sensitivity to parameters for malaria elimination. Trans R Soc Trop Med Hyg 110, 107–117. 10.1093/trstmh/trv113. [PubMed: 26822603]
8. Lazzari CR (2020). In the heat of the night. Science 367, 628–629. 10.1126/science.aba4484. [PubMed: 32029616]
9. Carde RT (2015). Multi-Cue Integration: How Female Mosquitoes Locate a Human Host. Current biology : CB 25, R793–795. 10.1016/j.cub.2015.07.057. [PubMed: 26394099]

10. Konopka JK, Task D, Afify A, Raji J, Deibel K, Maguire S, Lawrence R, and Potter CJ (2021). Olfaction in Anopheles mosquitoes. Chem Senses 46, bjab021. 10.1093/chemse/bjab021. [PubMed: 33885760]
11. Greppi C, Laursen WJ, Budelli G, Chang EC, Daniels AM, van Giesen L, Smidler AL, Catteruccia F, and Garrity PA (2020). Mosquito heat seeking is driven by an ancestral cooling receptor. Science 367, 681–684. 10.1126/science.aay9847. [PubMed: 32029627]
12. Lewis HE, Foster AR, Mullan BJ, Cox RN, and Clark RP (1969). Aerodynamics of the human microenvironment. Lancet 1, 1273–1277. 10.1016/s0140-6736(69)92220-x. [PubMed: 4182176]
13. Craven BA, and Settles GS (2006). A computational and experimental investigation of the human thermal plume. Journal of Fluids Engineering 128, 1251–1258.
14. Brown AWA, Sarkaria DS, and Thompson RP (1951). Studies on the responses of the female Aedes mosquito. Part I. The search for attractant vapours. Bull Entomol Res 42, 105–114.
15. Laarman JJ (1958). The host-seeking behavior of Anopheline mosquitoes. Geogr. Med. 10, 293–305.
16. Ismail IAH (1962). Sense Organs in the Antennae of Anopheles Maculipennis Atroparvus (v. THIEL), and their Possible Function in Relation to the Attraction of Female Mosquito to Man. Acta tropica 19, 1–58.
17. Takken W, Knols BG, and Otten H (1997). Interactions between physical and olfactory cues in the host-seeking behavior of mosquitoes: the role of relative humidity. Annals of Tropical Medicine and Parasitology 91 (1), S119–S120. 10.1080/00034983.1997.11813251.
18. McIver SB (1982). Sensilla mosquitoes (Diptera: Culicidae). J Med Entomol 19, 489–535. [PubMed: 6128422]
19. Altner H, and Loftus R (1985). Ultrastructure and function of insect thermo- and hygroreceptors. Ann. Rev. Entomol 30, 273–295.
20. Tichy H, and Gingl E (2001). Problems in hygro- and thermoreception. In The ecology of sensing, Barth FG, and Schimd A, eds. (Springer), pp. 271–287.
21. Tichy H (2007). Humidity-dependent cold cells on the antenna of the stick insect. J Neurophysiol 97, 3851–3858. [PubMed: 17392413]
22. Tichy H, and Kallina W (2010). Insect hygroreceptor responses to continuous changes in humidity and air pressure. J Neurophysiol 103, 3274–3286. 10.1152/jn.01043.2009. [PubMed: 20375249]
23. Knecht ZA, Silbering AF, Ni L, Klein M, Budelli G, Bell R, Abuin L, Ferrer AJ, Samuel AD, Benton R, and Garrity PA (2016). Distinct combinations of variant ionotropic glutamate receptors mediate thermosensation and hygrosensation in Drosophila. eLife 5. 10.7554/eLife.17879.
24. Knecht ZA, Silbering A, Cruz J, Yang L, Croset V, Benton R, and Garrity PA (2017). Ionotropic Receptor-dependent moist and dry cells control hygrosensation in Drosophila. eLife 6. 10.7554/eLife.26654.
25. Enjin A, Zaharieva EE, Frank DD, Mansourian S, Suh GS, Gallio M, and Stensmyr MC (2016). Humidity sensing in Drosophila. Current biology : CB 26, 1352–1358. 10.1016/j.cub.2016.03.049. [PubMed: 27161501]
26. Frank DD, Enjin A, Jouandet GC, Zaharieva EE, Para A, Stensmyr MC, and Gallio M (2017). Early intergration of temperature and humidity stimuli in the Drosophila brain. Current Biology 27, 1–8. 10.1016/j.cub.2017.06.077. [PubMed: 27916526]
27. Shanbhag SR, Singh K, and Singh RN (1995). Fine structure and primary sensory projections of sensilla located in the sacculus of the antenna of Drosophila melanogaster. Cell Tissue Res 282, 237–249. [PubMed: 8565054]
28. Marin EC, Buld L, Theiss M, Sarkissian T, Roberts RJV, Turnbull R, Tamimi IFM, Pleijzier MW, Laursen WJ, Drummond N, et al. (2020). Connectomics Analysis Reveals First-, Second-, and Third-Order Thermosensory and Hygrosensory Neurons in the Adult Drosophila Brain. Current biology : CB. 10.1016/j.cub.2020.06.028.
29. Kellogg FE (1970). Water vapour and carbon dioxide receptors in Aedes aegypti. J Insect Physiol 16, 99–108. 10.1016/0022-1910(70)90117-4. [PubMed: 5417711]
30. van den Broek IVF, and den Otter CJ (2000). Odour sensitivity of antennal olfactory cells underlying grooved pegs of Anopheles gambiae s.s. and An. quadriannulatus. Entomologia Experimentalis et Applicata 96, 167–175.

31. Davis EE (1977). Response of the antennal receptors of the male Aedes aegypti mosquito. J. Insect Physiol. 23, 613–617.
32. Budelli G, Ni L, Berciu C, van Giesen L, Knecht ZA, Chang EC, Kaminski B, Silbering AF, Samuel A, Klein M, et al. (2019). Ionotropic Receptors Specify the Morphogenesis of Phasic Sensors Controlling Rapid Thermal Preference in Drosophila. Neuron 101, 738–747 e733. 10.1016/j.neuron.2018.12.022. [PubMed: 30654923]
33. Grimaldi D, and Engel MS (2005). Evolution of the insects (Cambridge University Press).
34. Clements AN (1999). The Biology of Mosquitoes: Development, Nutrition and Reproduction (CABI Publishing).
35. Okal MN, Francis B, Herrera-Varela M, Fillinger U, and Lindsay SW (2013). Water vapour is a pre-oviposition attractant for the malaria vector Anopheles gambiae sensu stricto. Malar J 12, 365. 10.1186/1475-2875-12-365. [PubMed: 24120083]
36. Day JF (2016). Mosquito Oviposition Behavior and Vector Control. Insects 7. 10.3390/insects7040065.
37. Matthews BJ, Younger MA, and Vosshall LB (2019). The ion channel ppk301 controls freshwater egg-laying in the mosquito Aedes aegypti. eLife 8. 10.7554/eLife.43963.
38. Fillinger U, Sombroek H, Majambere S, van Loon E, Takken W, and Lindsay SW (2009). Identifying the most productive breeding sites for malaria mosquitoes in The Gambia. Malar J 8, 62. 10.1186/1475-2875-8-62. [PubMed: 19361337]
39. Morrison AC, Gray K, Getis A, Astete H, Sihuincha M, Focks D, Watts D, Stancil JD, Olson JG, Blair P, and Scott TW (2004). Temporal and geographic patterns of Aedes aegypti (Diptera: Culicidae) production in Iquitos, Peru. J Med Entomol 41, 1123–1142. 10.1603/0022-2585-41.6.1123. [PubMed: 15605653]
40. Kraemer MU, Sinka ME, Duda KA, Mylne AQ, Shearer FM, Barker CM, Moore CG, Carvalho RG, Coelho GE, Van Bortel W, et al. (2015). The global distribution of the arbovirus vectors Aedes aegypti and Ae. albopictus. eLife 4, e08347. 10.7554/eLife.08347. [PubMed: 26126267]
41. Benton R, Vannice KS, Gomez-Diaz C, and Vosshall LB (2009). Variant ionotropic glutamate receptors as chemosensory receptors in Drosophila. Cell 136, 149–162. [PubMed: 19135896]
42. Croset V, Rytz R, Cummins SF, Budd A, Brawand D, Kaessmann H, Gibson TJ, and Benton R (2010). Ancient protostome origin of chemosensory ionotropic glutamate receptors and the evolution of insect taste and olfaction. PLoS Genet 6, e1001064. 10.1371/journal.pgen.1001064. [PubMed: 20808886]
43. Miller DE, Cook KR, and Hawley RS (2019). The joy of balancers. PLoS Genet 15, e1008421. 10.1371/journal.pgen.1008421. [PubMed: 31697682]
44. Pitts RJ, Rinker DC, Jones PL, Rokas A, and Zwiebel LJ (2011). Transcriptome profiling of chemosensory appendages in the malaria vector Anopheles gambiae reveals tissue- and sex-specific signatures of odor coding. BMC Genomics 12, 271. 10.1186/1471-2164-12-271. [PubMed: 21619637]
45. Riabinina O, Task D, Marr E, Lin CC, Alford R, O'Brochta DA, and Potter CJ (2016). Organization of olfactory centres in the malaria mosquito Anopheles gambiae. Nature communications 7, 13010. 10.1038/ncomms13010.
46. Pitts RJ, and Zwiebel LJ (2006). Antennal sensilla of two female anopheline sibling species with differing host ranges. Malar J 5, 26. 10.1186/1475-2875-5-26. [PubMed: 16573828]
47. Afify A, Betz JF, Riabinina O, Lahondere C, and Potter CJ (2019). Commonly Used Insect Repellents Hide Human Odors from Anopheles Mosquitoes. Current biology : CB 29, 3669–3680 e3665. 10.1016/j.cub.2019.09.007. [PubMed: 31630950]
48. Zhao Z, Tian D, and McBride CS (2021). Development of a pan-neuronal genetic driver in Aedes aegypti mosquitoes. Cell Rep Methods 1. 10.1016/j.crmeth.2021.100042.
49. Powell JR, Gloria-Soria A, and Kotsakiozi P (2018). Recent History of Aedes aegypti: Vector Genomics and Epidemiology Records. Bioscience 68, 854–860. 10.1093/biosci/biy119. [PubMed: 30464351]
50. van Giesen L, and Garrity PA (2017). More than meets the IR: the expanding roles of variant Ionotropic Glutamate Receptors in sensing odor, taste, temperature and moisture. F1000Res 6, 1753. 10.12688/f1000research.12013.1. [PubMed: 29034089]

51. Ni L (2021). The Structure and Function of Ionotropic Receptors in Drosophila. Frontiers in molecular neuroscience 13, 638839. 10.3389/fnmol.2020.638839. [PubMed: 33597847]
52. Auer TO, Khallaf MA, Silbering AF, Zappia G, Ellis K, Alvarez-Ocana R, Arguello JR, Hansson BS, Jefferis G, Caron SJC, et al. (2020). Olfactory receptor and circuit evolution promote host specialization. Nature 579, 402–408. 10.1038/s41586-020-2073-7. [PubMed: 32132713]
53. Eyun SI, Soh HY, Posavi M, Munro JB, Hughes DST, Murali SC, Qu J, Dugan S, Lee SL, Chao H, et al. (2017). Evolutionary History of Chemosensory-Related Gene Families across the Arthropoda. Mol Biol Evol 34, 1838–1862. 10.1093/molbev/msx147. [PubMed: 28460028]
54. Kozma MT, Schmidt M, Ngo-Vu H, Sparks SD, Senatore A, and Derby CD (2018). Chemoreceptor proteins in the Caribbean spiny lobster, Panulirus argus: Expression of Ionotropic Receptors, Gustatory Receptors, and TRP channels in two chemosensory organs and brain. PloS one 13, e0203935. 10.1371/journal.pone.0203935. [PubMed: 30240423]
55. Li S, Li B, Gao L, Wang J, and Yan Z (2022). Humidity response in Drosophila olfactory sensory neurons requires the mechanosensitive channel TMEM63. Nature communications 13, 3814. 10.1038/s41467-022-31253-z.
56. Chappuis CJ, Beguin S, Vlimant M, and Guerin PM (2013). Water vapour and heat combine to elicit biting and biting persistence in tsetse. Parasit Vectors 6, 240. 10.1186/1756-3305-6-240. [PubMed: 23958224]
57. Gatehouse AG (1970). The probing response of Stomoxys calcitrans to certain physical and olfactory stimuli. J. Insect Physiol. 16, 61–74. [PubMed: 5417708]
58. Barrozo RB, Manrique G, and Lazzari CR (2003). The role of water vapour in the orientation behaviour of the blood-sucking bug Triatoma infestans (Hemiptera, Reduviidae). J Insect Physiol 49, 315–321. 10.1016/s0022-1910(03)00005-2. [PubMed: 12769985]
59. Wiegmann BM, Trautwein MD, Winkler IS, Barr NB, Kim JW, Lambkin C, Bertone MA, Cassel BK, Bayless KM, Heimberg AM, et al. (2011). Episodic radiations in the fly tree of life. Proceedings of the National Academy of Sciences of the United States of America 108, 5690–5695. 10.1073/pnas.1012675108. [PubMed: 21402926]
60. Xiao R, and Xu XZS (2021). Temperature sensation: from molecular thermosensors to neural circuits and coding principles. Annual Review of Physiology 83, 205–230. 10.1146/annurev-physiol-031220-095215.
61. McMeniman CJ, Corfas RA, Matthews BJ, Ritchie SA, and Vosshall LB (2014). Multimodal integration of carbon dioxide and other sensory cues drives mosquito attraction to humans. Cell 156, 1060–1071. 10.1016/j.cell.2013.12.044. [PubMed: 24581501]
62. Brown AWA (1966). The attraction of mosquitoes to hosts. Journal of the American Medical Association 196, 159–162. [PubMed: 5952113]
63. Howlett FM (1910). The influence of temperature upon the biting of mosquitoes. Parasitology 3, 479–484.
64. Burgess L (1959). Probing behavior of Aedes aegypti (L.) in response to heat and moisture. Nature 184, 1968–1969.
65. Reinhold JM, Chandrasegaran K, Oker H, Crespo JE, Vinauger C, and Lahondere C (2022). Species-Specificity in Thermopreference and CO2-Gated Heat-Seeking in Culex Mosquitoes. Insects 13. 10.3390/insects13010092.
66. Coutinho-Abreu IV, Clark JT, and Ray A (2022). Pentylamine inhibits humidity detection in insect vectors of human and plant borne pathogens. Sci Rep 12, 16732. 10.1038/s41598-022-20488-x. [PubMed: 36202886]
67. Giribet G, and Edgecombe GD (2019). The Phylogeny and Evolutionary History of Arthropods. Current biology : CB 29, R592–R602. 10.1016/j.cub.2019.04.057. [PubMed: 31211983]
68. Penalver E, Arillo A, Delclos X, Peris D, Grimaldi DA, Anderson SR, Nascimbene PC, and Fuente RP (2018). Ticks parasitised feathered dinosaurs as revealed by Cretaceous amber assemblages. Nature communications 9, 472. 10.1038/s41467-018-02913-w.
69. Otálora-Luna F, Pérez-Sánchez AJ, Sandoval C, and Aldana E (2015). Evolution of hematophagous habit in Triatominae (Heteroptera: Reduviidae). Revista Chilena de Historia Natural 88, 4. 10.1186/s40693-014-0032-0.

70. Rota-Stabelli O, Daley AC, and Pisani D (2013). Molecular timetrees reveal a Cambrian colonization of land and a new scenario for ecdysozoan evolution. Current biology : CB 23, 392–398. [PubMed: 23375891]

71. Matthews BJ, Dudchenko O, Kingan SB, Koren S, Antoshechkin I, Crawford JE, Glassford WJ, Herre M, Redmond SN, Rose NH, et al. (2018). Improved reference genome of Aedes aegypti informs arbovirus vector control. Nature 563, 501–507. 10.1038/s41586-018-0692-z. [PubMed: 30429615]

72. Li M, Yang T, Kandul NP, Bui M, Gamez S, Raban R, Bennett J, Sanchez CH, Lanzaro GC, Schmidt H, et al. (2020). Development of a confinable gene drive system in the human disease vector Aedes aegypti. eLife 9. 10.7554/eLife.51701.

73. Li M, Bui M, Yang T, Bowman CS, White BJ, and Akbari OS (2017). Germline Cas9 expression yields highly efficient genome engineering in a major worldwide disease vector, Aedes aegypti. Proceedings of the National Academy of Sciences of the United States of America 114, E10540–E10549. 10.1073/pnas.1711538114. [PubMed: 29138316]

74. Volohonsky G, Terenzi O, Soichot J, Naujoks DA, Nolan T, Windbichler N, Kapps D, Smidler AL, Vittu A, Costa G, et al. (2015). Tools for Anopheles gambiae Transgenesis. G3 (Bethesda) 5, 1151–1163. 10.1534/g3.115.016808. [PubMed: 25869647]

75. Zhang Y, Werling U, and Edelmann W (2014). Seamless Ligation Cloning Extract (SLiCE) cloning method. Methods Mol Biol 1116, 235–244. 10.1007/978-1-62703-764-8_16. [PubMed: 24395368]

76. Butterwick JA, Del Marmol J, Kim KH, Kahlson MA, Rogow JA, Walz T, and Ruta V (2018). Cryo-EM structure of the insect olfactory receptor Orco. Nature 560, 447–452. 10.1038/s41586-018-0420-8. [PubMed: 30111839]

77. Younger MA, Herre M, Ehrlich AR, Gong Z, Gilbert ZN, Rahiel S, Matthews BJ, and Vosshall LB (2020). Non-canonical odor coding ensures unbreakable mosquito attraction to humans. bioRxiv. 10.1101/2020.11.07.368720

78. Maguire SE, Afify A, Goff LA, and Potter CJ (2022). Odorant-receptor-mediated regulation of chemosensory gene expression in the malaria mosquito Anopheles gambiae. Cell Rep 38, 110494. 10.1016/j.celrep.2022.110494. [PubMed: 35263579]

79. Thevenaz P, Ruttimann UE, and Unser M (1998). A pyramid approach to subpixel registration based on intensity. IEEE Trans Image Process 7, 27–41. 10.1109/83.650848. [PubMed: 18267377]

Highlights:

- Mosquitoes sense heat and humidity via Ionotropic Receptor *Ir93a*-dependent sensors
- *Ir93a*-dependent sensors promote detection of human host proximity and blood feeding
- Gravid females require *Ir93a* to seek high humidity associated with egg-laying sites
- Both *An. gambiae* and *Ae. aegypti* rely on *Ir93a* to blood feed and locate egg-lay sites

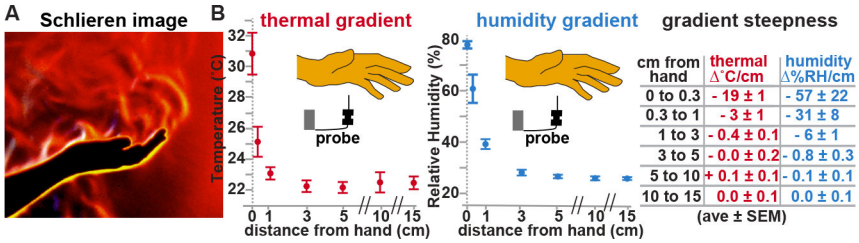

Figure 1: Humans generate co-extensive thermal and humidity gradients.

(A) Schlieren image revealing refractive index variations near hand, reflecting variations in temperature and humidity. Yellow/white, inner boundary layer. Image, G. Settles; for details on Schlieren imaging [13]. **(B)** Gradients beneath hand. n=6.

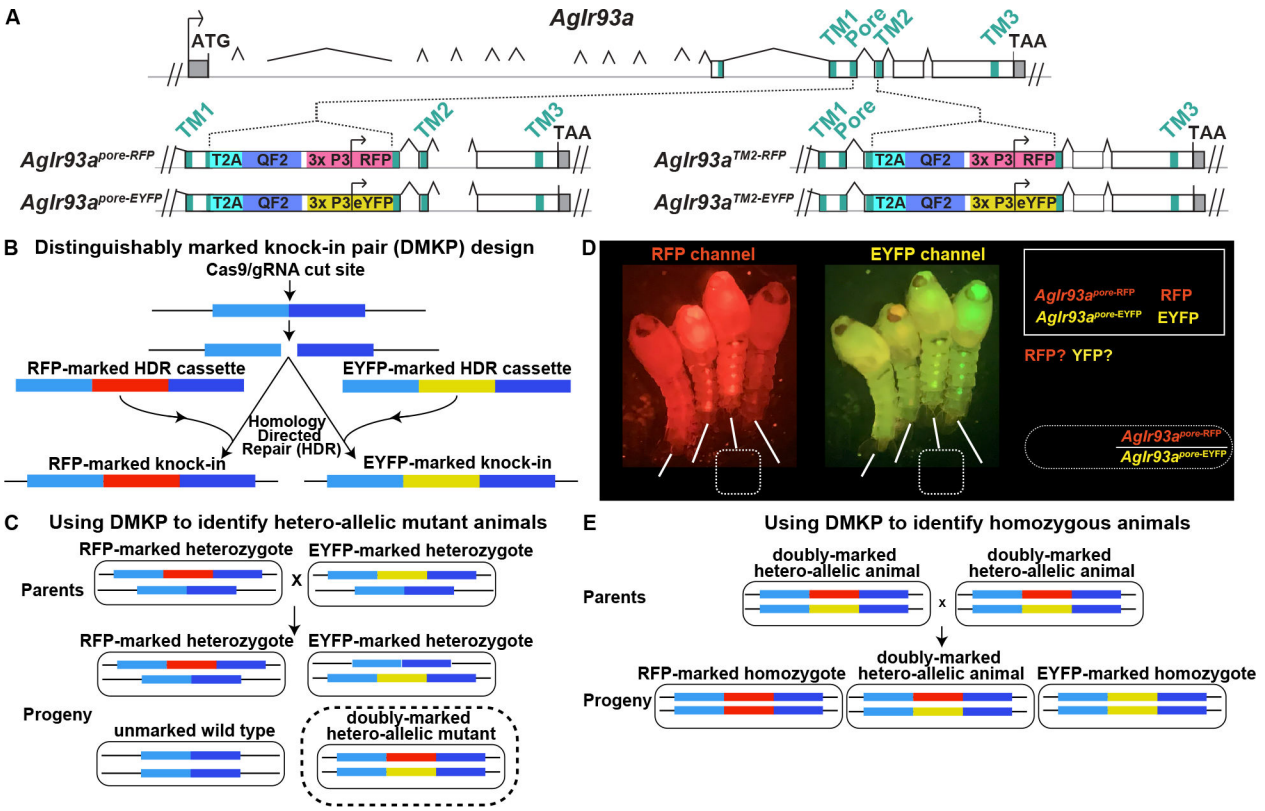

Figure 2: *AgIr93a* QF2 knock-in animals and the Distinguishably Marked Knock-in Pair (DMKP) strategy.

(**A**) Top depicts *AgIr93a* locus organization. Exonic regions encoding the three transmembrane domains and ion pore are denoted in blue-green. 5' and 3' UTR are gray. Bottom panels depicts gene structure in $AgIr93a^{pore}$ and in $AgIr93a^{TM2}$ alleles. Each allele was produced by insertion of a knock-in cassette at the location indicated. T2A sequences allow expression of two independent polypeptides from a single mRNA, permitting the expression of the QF2 transcription factor as a separate polypeptide from a transcript initiated at the endogenous *AgIr93a* start site. The 3xP3 promoter was used to drive visual system and ventral cord expression of the fluorescent transformation marker, which was either RFP or EYFP. **(B)** Generation of two knock-ins at the same genomic position, identical except that one knock-in is marked with RFP and the other with EYFP. (**C**) Creating a distinguishably marked hetero-allelic mutant animal using the DMKP strategy. (**D**) $AgIr93a^{pore}$ DMKP pupae. Note that the $AgIr93a^{pore\text{-}RFP}/AgIr93a^{pore\text{-}EYFP}$ hetero-allelic mutant pupae express both RFP and EYFP, while heterozygotes and wild type animals do not. Arrowheads highlight RFP and EYFP expression patterns. (**E**) Generating reliably homozygous knock-in strains by interbreeding hetero-allelic parents using DMKP.

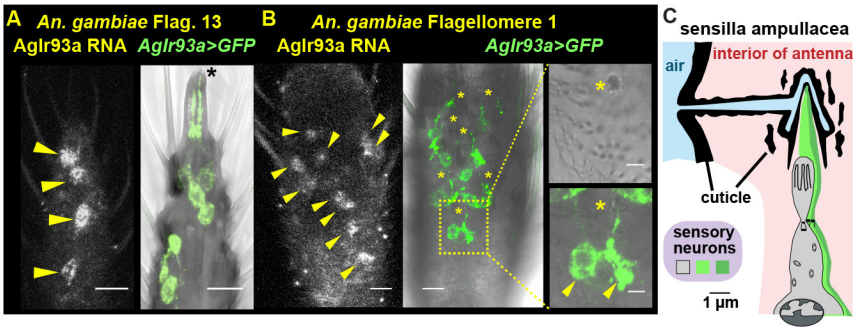

Figure 3: Mosquitoes express *AgIr93a>CD8:GFP* in potential thermo- and hygro-sensors.

(A, B) *AgIr93a* RNA in situ and Ag*Ir93a*$^{pore\text{-}RFP}$*>CD8:GFP*. Insets (right) highlight sensilla ampullacea (top), with CD8:GFP overlay (bottom). Yellow arrowheads, cell bodies. Black asterisk, coeloconic sensilla. Yellow asterisks, sensilla ampullacea. **(C)** Drawing after that in [18]. See also Figure S1.

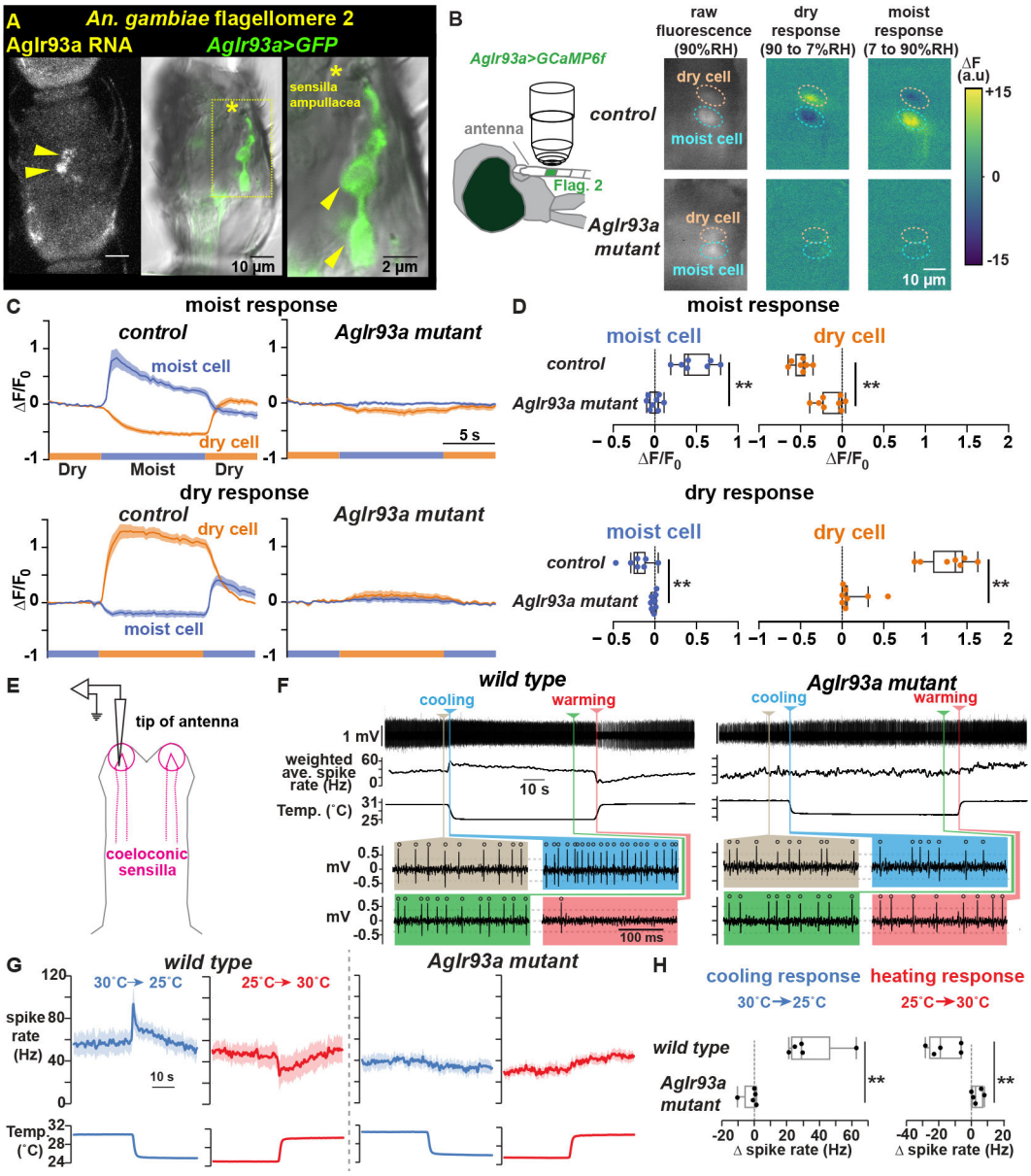

Figure 4: *AgIr93a* mediates hygrosensation and thermosensation.

(A) *AgIr93a* in situ and *AgIr93a*$^{pore\text{-}RFP}$>*CD8:GFP*-labeled neurons in flagellomere 2. Arrowheads, cell bodies. Asterisk, sensilla ampullacea opening. **(B)** Trans-cuticular imaging of *AgIr93a*$^{pore\text{-}RFP}$>*GCaMP6f* fluorescence and its change upon relative humidity (RH) shifts. Dashed ovals, soma. **(C)** Responses to RH shifts between 90% (moist) and 7% (dry). Mean +/− SEM. Control (*AgIr93a*$^{pore\text{-}RFP}$/+), n=7 animals. *AgIr93a* mutant (*AgIr93a*$^{pore\text{-}RFP}$/*AgIr93a*$^{pore\text{-}EYFP}$), n=8. F_0 = average 5.5s to 1s pre-stimulus-switch. **(D)** Fluorescence change upon switching between moist and dry. ΔF = F(average 3s to 5.5s post-switch) − F_0. ** p<0.001, t-test. **(E)** Coeloconic sensilla recording. **(F)** *wild type* (*G3*) and *AgIr93a* mutant (*AgIr93a*$^{TM2\text{-}RFP}$/*AgIr93a*$^{TM2\text{-}EYFP}$) recordings. Weighted average spike rates (1s triangular window). Colored panels highlight activity at indicated times. Open circles, spikes. Dashed lines, thresholds. **(G)** Peri-stimulus time histograms

(average +/− SEM). Cooling, blue. Warming, red. *wild type*, n=5 animals. *AgIr93a*$^{TM2\text{-}RFP}$/*AgIr93a*$^{TM2\text{-}EYFP}$, n=5. **(H)** Cooling response = (average Hz 0.2s-0.7s after cooling onset) – (average Hz 5s-10s pre-cooling). ** p=0.009, Wilcoxon. Heating response = (average Hz 0.5s-1.5s after heating onset) – (average Hz 5s-10s pre-heating). ** p= 0.0026, t-test.

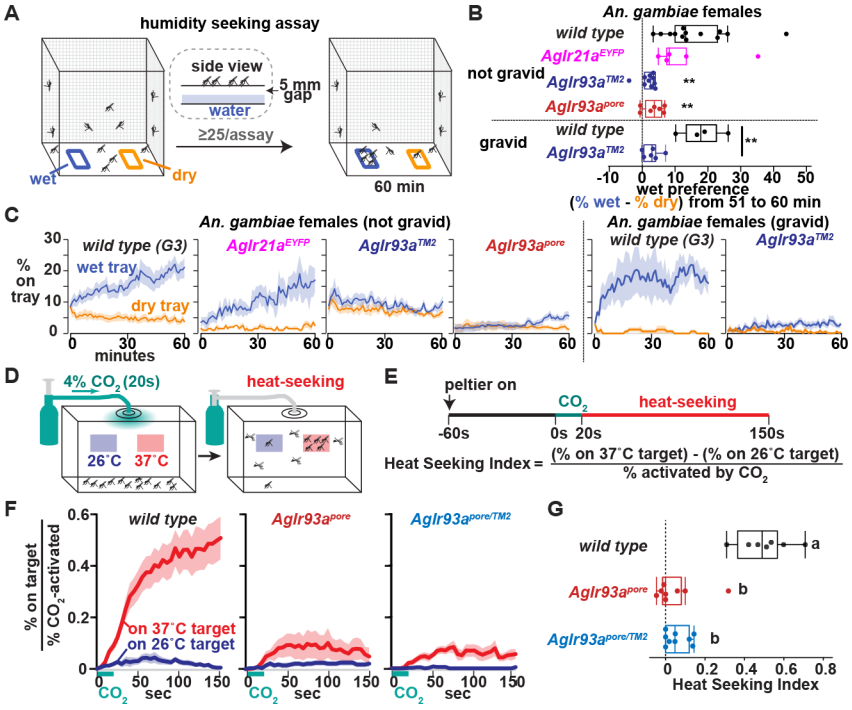

Figure 5: *AgIr93a* is required for humidity and heat seeking.

(A) Humidity-seeking assay. **(B)** Average (% on wet − % on dry) 51 to 60 min. Not gravid, **p<0.01 versus *wt*, Steel with control. Gravid, ** P<0.01, t-test. **(C)** Mosquitoes landed on trays. Mean +/− SEM. 25–73 females/assay. Not gravid: *wt*, n=13 assays. *AgIr21a*^{EYFP}, n=5. *AgIr93a*$^{TM2\text{-}RFP}$/*AgIr93a*$^{TM2\text{-}EYFP}$, n=10. *AgIr93a*$^{pore\text{-}RFP}$/*AgIr93a*$^{pore\text{-}EYFP}$, n=7. Gravid: *wt*, n=4 assays. *AgIr93a*$^{TM2\text{-}RFP}$/*AgIr93a*$^{TM2\text{-}EYFP}$, n=6. **(D)** Heat seeking assay. **(E)** Assay time-course and index calculation. **(F)** Fraction of CO_2-activated mosquitoes landed on targets. Average +/− SEM. Wild type, n=7 assays. *AgIr93a*$^{pore\text{-}RFP}$/*AgIr93a*$^{pore\text{-}EYFP}$, n=7. *AgIr93a*$^{pore\text{-}EYFP}$/*AgIr93a*$^{TM2\text{-}RFP}$, n=9. 46–50 females/assay. **(G)** Heat seeking index, average 130s-150s. Letters denote distinct groups, p<0.01, Steel-Dwass. See also Figure S2.

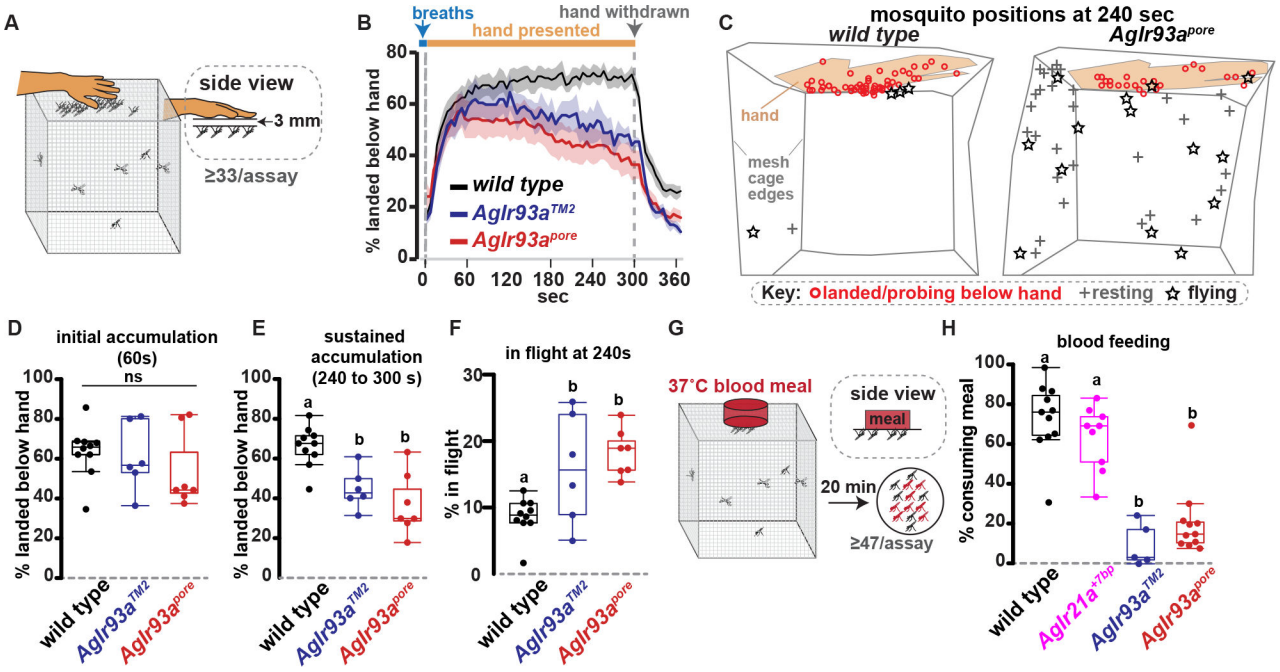

Figure 6: *AgIr93a* is required to maintain close-range host attraction and promote blood feeding.

(A) Host attraction assay. **(B)** Average +/− SEM. 41–76 females/assay. *wild type*, n=10 assays. *AgIr93a*$^{TM2\text{-}RFP}$/*AgIr93a*$^{TM2\text{-}EYFP}$, n=6. *AgIr93a*$^{pore\text{-}RFP}$/*AgIr93a*$^{pore\text{-}EYFP}$, n=7. **(C)** Tracings of mosquito locations and behaviors from assay videos 240s post-hand presentation. **(D-E)** Mosquitoes landed under hand 60s (ANOVA, p=0.851) (**D**) and 240–300s post-hand presentation (letters denote distinct groups, Tukey HSD, alpha=0.01) (**E**). **(F)** Animals in flight 240s post-hand presentation. Tukey HSD, alpha=0.05. **(G)** Blood feeding assay, with human blood meal behind collagen membrane. **(H)** Blood consumption. 47–76 females/assay. *wild type*, n=11 assays. *AgIr21a*$^{+7bp}$, n=9. *AgIr93a*$^{TM2-RFP}$/*AgIr93a*$^{TM2\text{-}EYFP}$, n=5. *AgIr93a*$^{pore\text{-}RFP}$/*AgIr93a*$^{pore\text{-}EYFP}$, n=11. Steel-Dwass, p<0.05. See also Movies 1 and 2 and Figure S3.

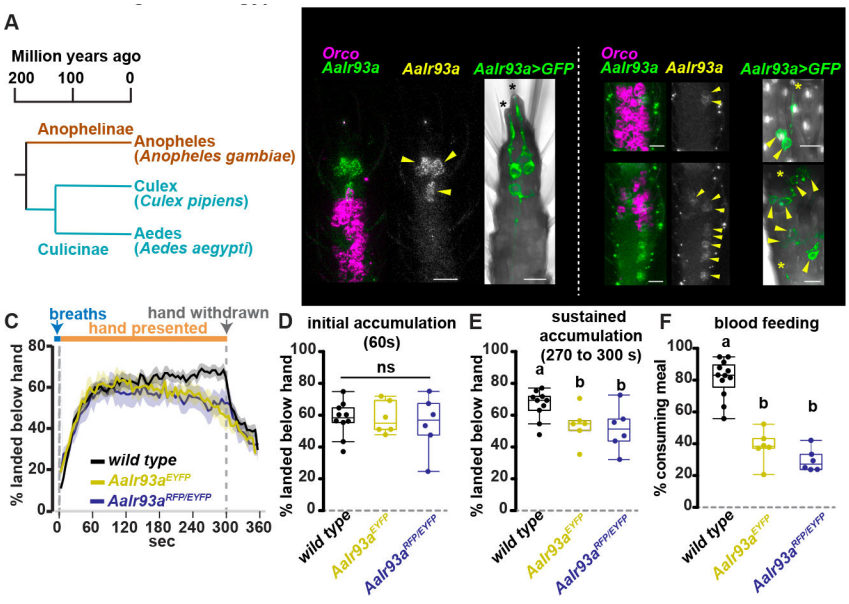

Figure 7: *Ir93a* is required to maintain close-range host attraction and promote blood feeding in *Ae. aegypti*. **(A)** Vector mosquito phylogeny. **(B)** *AaIr93a* and *AaOrco* RNA in situ and *AaIr93a*^{RFP}>*CD8:GFP* expression. Arrowheads, cell bodies. Black asterisks, coeloconic sensilla. Yellow asterisks, sensilla ampullacea. **(C)** Average +/− SEM. 51–63 females/assay. *wild type* (LVP), n=10 assays. *AaIr93a*^{EYFP}/*AaIr93a*^{EYFP}, n=6. *AaIr93a*^{RFP}/*AaIr93a*^{EYFP}, n=6. (**D-E**) Mosquitoes landed under hand 60s (ANOVA, p=0.89) (**D**) and 270–300s post-hand presentation (letters denote distinct groups, Tukey HSD, alpha=0.05) (**E**). **(F)** Blood meal consumption. 51–63 females/assay. *wild type*, n=12 assays. *AaIr93a*^{EYFP}/*AaIr93a*^{EYFP}, n=6. *AaIr93a*^{RFP}/*AaIr93a*^{EYFP}, n=6. (letters denote distinct groups, Tukey HSD, alpha=0.01). See also Figures S4–S5.

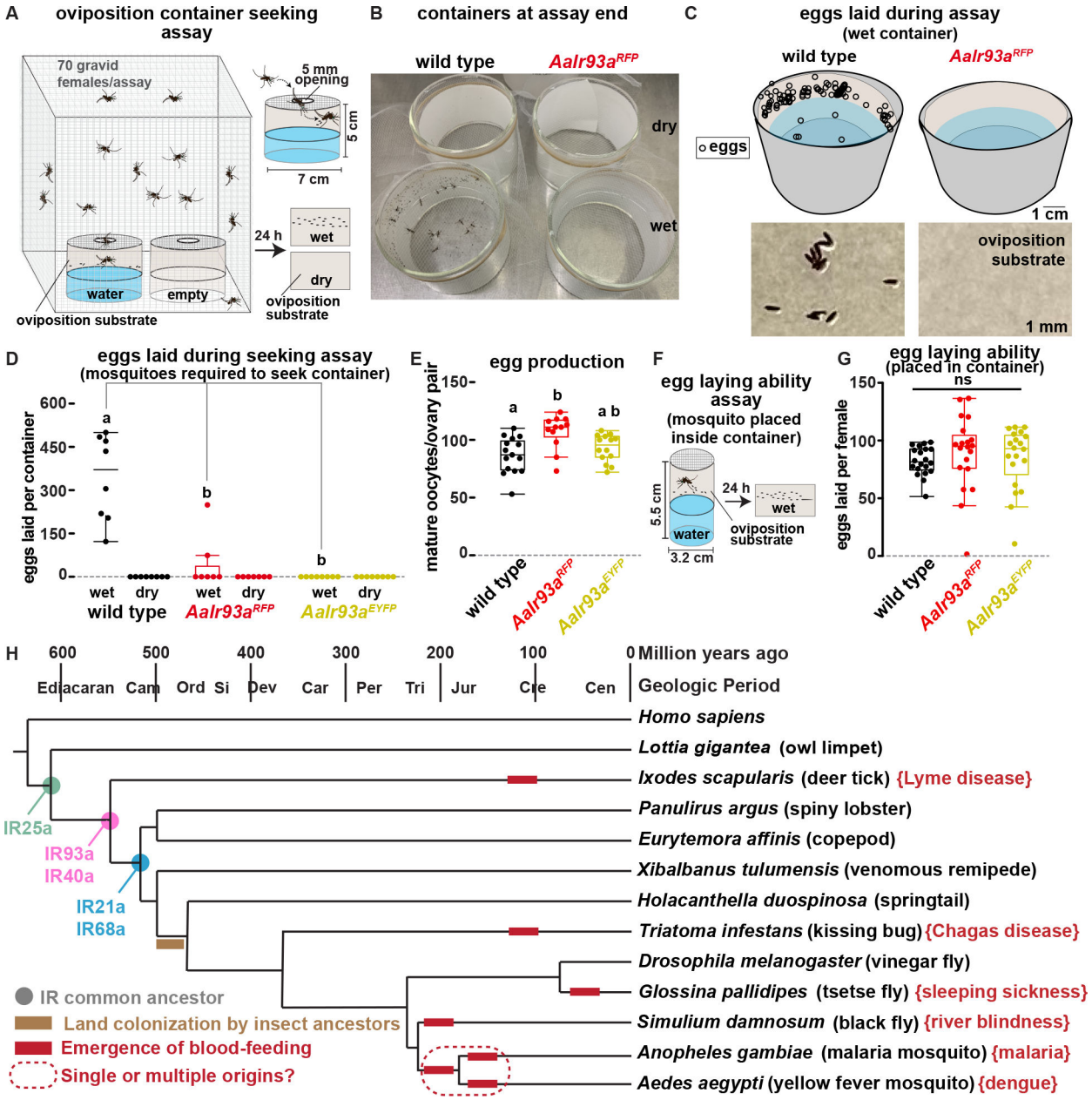

Figure 8: *Ir93a* promotes oviposition site attraction in *Ae. aegypti* and is conserved among arthropods.

(A) Oviposition site selection assay. **(B)** Potential oviposition site containers at assay end, with mosquitoes and eggs present only in *wild type*, wet container. **(C)** Upper panel, egg deposition in wet containers by assay end. Lower panel, photograph of portion of oviposition substrate from wet container. **(D)** Quantitation of egg deposition in seeking assay. 70 gravid females/assay. *wild type* (LVP), n=8 assays. $AaIr93a^{RFP}/AaIr93a^{RFP}$, n=7. $AaIr93a^{EYFP}/AaIr93a^{EYFP}$, n=8. Letters denote distinct groups, comparisons among wet containers. Steel-Dwass p≤0.01. (**E**) Mature oocytes present in dissected ovaries of gravid females. Letters denote distinct groups, Steel-Dwass p≤0.02. (**F**) Egg-laying ability assay. (**G**) Eggs laid by single gravid females placed in a water-containing oviposition chamber.

n=20 individuals/genotype. Kruskal-Wallis, p =0.18. (**H**) Ionotropic Receptor distribution. Cladogram, land colonization and blood-feeding emergence times based on [33,59,67–70]. Cam, Cambrian. Ord, Ordovician. Si, Silurian. Dev, Devonian. Car, Carboniferous. Per, Permian. Tri, Triassic. Jur, Jurassic. Cre, Cretaceous. Cen, Cenozoic (era). Brackets note a disease transmitted by each vector. See also Figure S6.

Key resources table

REAGENT or RESOURCE	SOURCE	IDENTIFIER
Antibodies		
Chicken anti-GFP	Aves Labs	Cat# GFP-1010; RRID: AB_2307313
Mouse anti-*Apocrypta bakeri* Orco	Laboratory of Vanessa Ruta Butterwick et al. [76]	15B2
Goat anti-mouse Cy5	Invitrogen	Cat# A10524; RRID: AB_2534033
Goat anti-chicken Alexa Fluor 488	Invitrogen	Cat# A11039; RRID: AB_2534096
Bacterial and virus strains		
Biological samples		
Chemicals, peptides, and recombinant proteins		
Critical commercial assays		
HCR RNA in situ probes, amplifiers, buffers; see DataS1 for additional details	Molecular Instruments	https://www.molecularinstruments.com/
Deposited data		
Experimental models: Cell lines		
Experimental models: Organisms/strains		
Anopheles gambiae: Wild-type *G3* strain	Laboratory of Flaminia Catteruccia Greppi et al.[11]	N/A
Anopheles coluzzii: QUAS-mCD8:GFP strain	Laboratory of Christopher Potter Riabinina et al.[45]	N/A
Anopheles coluzzii: QUAS-GCAMP6f strain	Laboratory of Christopher Potter Afify et al.[47]	N/A
Anopheles gambiae: Ir93a^{pore}-T2A-Qf2-3xP3-RFP strain	This paper	N/A
Anopheles gambiae: Ir93a^{pore}-T2A-Qf2-3xP3-eYFP strain	This paper	N/A
Anopheles gambiae: Ir93a^{TM2}-T2A-Qf2-3xP3-RFP strain	This paper	N/A
Anopheles gambiae: Ir93a^{TM2}-T2A-Qf2-3xP3-eYFP strain	This paper	N/A
Anopheles gambiae: Ir21a^{eYFP} strain	Garrity lab Greppi et al.[11]	N/A
Anopheles gambiae: Ir21a^{+7bp} strain	Garrity lab Greppi et al.[11]	N/A
Aedes aegypti: Wild-type Liverpool (*LVP*) strain	Laboratory of Leslie Vosshall Matthews et al.[71]	N/A
Aedes aegypti: QUAS-mCD8:GFP strain	Laboratory of Carolyn McBride Matthews et al.[37]	N/A
Aedes aegypti: QUAS-GCAMP7s-T2A-tdTomato strain	Laboratory of Carolyn McBride Zhao et al.[48]	N/A
Aedes aegypti: Ir93a-T2A-Qf2-3xP3-RFP strain	This paper	N/A
Aedes aegypti: Ir93a-T2A-Qf2-3xP3-eYFP strain	This paper	N/A
Oligonucleotides		
See DataS1 for assembled list of oligonucleotide sequences	This paper	N/A
Recombinant DNA		

REAGENT or RESOURCE	SOURCE	IDENTIFIER
Plasmid: AgIr93a^{pore}-T2A-Qf2-3xP3-RFP HDR	This paper	N/A
Plasmid: AgIr93a^{pore}-T2A-Qf2-3xP3-eYFP HDR	This paper	N/A
Plasmid: AgIr93a^{TM2}-T2A-Qf2-3xP3-RFP HDR	This paper	N/A
Plasmid: AgIr93a^{TM2}-T2A-Qf2-3xP3-eYFP HDR	This paper	N/A
Plasmid: AaIr93a-T2A-Qf2-3xP3-RFP HDR	This paper	N/A
Plasmid: AaIr93a-T2A-Qf2-3xP3-eYFP HDR	This paper	N/A
Plasmid: AgU6C-Ir93a-pore-gRNA-AgVasa-Cas9	This paper	N/A
Plasmid: AgU6C-Ir93a-TM2-gRNA-AgVasa-Cas9	This paper	N/A
Plasmid: AaU6C-Ir93a-gRNA-AaExu-Cas9	This paper	N/A
Software and algorithms		
Fiji (2.3.0/1.5.3f)	ImageJ	https://imagej.net/software/fiji/ RRID:SCR_002285
Photoshop (21.2.2)	Adobe	https://www.adobe.com/ RRID:SCR_014199
Illustrator (24.2.3)	Adobe	https://www.adobe.com/ RRID:SCR_010279
JMP 11	SAS	https://www.jmp.com/ RRID:SCR_014242
LabChart Pro V7	AD Instruments	https://www.adinstruments.com/ RRID:SCR_017551
GraphPad Prism 9	GraphPad	https://www.graphpad.com/ RRID:SCR_002798
Stackreg	Thevenaz et al.[79]	http://bigwww.epfl.ch/thevenaz/stackreg/
Other		